NACA RM A55D11

RESEARCH MEMORANDUM

INVESTIGATION OF THE EFFECTS OF AN AIRFOIL SECTION MODIFICATION ON THE AERODYNAMIC CHARACTERISTICS AT SUBSONIC AND SUPERSONIC SPEEDS OF A THIN SWEPT WING OF ASPECT RATIO 3 IN COMBINATION WITH A BODY

By David Graham and William T. Evans

Ames Aeronautical Laboratory
Moffett Field, Calif.

NATIONAL ADVISORY COMMITTEE
FOR AERONAUTICS

WASHINGTON

June 28, 1955
Declassified February 26, 1958

NATIONAL ADVISORY COMMITTEE FOR AERONAUTICS

RESEARCH MEMORANDUM

INVESTIGATION OF THE EFFECTS OF AN AIRFOIL SECTION MODIFICATION ON THE AERODYNAMIC CHARACTERISTICS AT SUBSONIC AND SUPERSONIC SPEEDS OF A THIN SWEPT WING OF ASPECT RATIO 3 IN COMBINATION WITH A BODY

By David Graham and William T. Evans

SUMMARY

A wind-tunnel investigation has been conducted to determine the effects of an airfoil section modification consisting of a greatly increased leading-edge radius and slight forward camber on the aerodynamic characteristics of a thin swept-wing-body combination at Mach numbers from 0.06 to 1.9. The basic wing had an aspect ratio of 3, taper ratio of 0.4, leading-edge sweep of 45°, and an NACA 64A006 airfoil section perpendicular to the quarter-chord line. A large-scale model was tested at low speeds and at Reynolds numbers from 4.4×10^6 to 21×10^6 and a small-scale model was tested at high subsonic and supersonic speeds at Reynolds numbers from 2.9×10^6 to 5.7×10^6. Lift, drag, and pitching moment were measured.

The tests showed that full-span modification of the wing resulted in very marked improvement in stability, drag, and high-lift characteristics for the configuration at low speeds, due to the maintenance of attached flow over the wing to high lift coefficients. At high speeds, although the modification resulted in less drag at the higher lift coefficients, there was a drag penalty at low lift coefficients, which was especially serious at supersonic Mach numbers.

Computation by linearized supersonic theory of the wave drag at zero lift at Mach numbers of 1.00 and 1.28 for both the basic and modified wing-body combinations, the effect of camber being neglected, indicated that a significant part of the drag increment was traceable to the change of area distribution associated with the modified wing.

In addition to full-span modification of the wing, a partial-span modification was tested at low speed. Split flaps were tested at low speed on the model with full-span wing modifications.

The detailed derivation of the modified airfoil section is presented together with low-speed two-dimensional test results for the modified airfoil section. Comparisons are also made between measured low-speed drag and stability "breaks" and those predicted by simple-sweep theory applied to the two-dimensional characteristics.

INTRODUCTION

The adverse effects of wing-tip stall on the low-speed stability and drag characteristics of swept-wing airplanes are widely recognized. To delay wing-tip stall to higher lift coefficients, the use of large increases in leading-edge radius together with slight amounts of forward camber has been shown to be effective on wings of moderate thickness (refs. 1 to 3). However, there appear to be little data on the high-speed effects of such modifications on wing-body combinations, and not any data at all on their effects on thin wings.

The purpose of the investigation reported herein was to evaluate the effects of such a modification on a thin swept wing of low aspect ratio in combination with a body at both subsonic and supersonic speeds. The modified airfoil section was designed to attain a given low-speed $c_{l_{max}}$, comparable to that which might be expected from leading-edge flaps. The experimental three-dimensional results, obtained at several Reynolds numbers, are presented and discussed from both the low-speed and high-speed standpoints. The measured low-speed characteristics are compared with predictions based on simple-sweep theory applied to the two-dimensional wing section characteristics. The measured transonic drag rise at zero lift is compared with values of wave drag computed by linearized theory.

NOTATION

A	aspect ratio, $\frac{b^2}{S}$
C_D	drag coefficient, $\frac{\text{drag}}{qS}$
C_{D_o}	drag coefficient at zero lift
C_{D_o}'	zero lift wave-drag coefficient, $\frac{\text{theoretical wave drag at zero lift}}{qS}$
$\left(C_{D_o}'\right)_M$	zero lift wave-drag coefficient due to wing modification, taken as difference in C_{D_o}' between modified and unmodified configurations

ΔC_{D_o} zero lift drag-rise coefficient, (C_{D_o} at M>1) - (C_{D_o} at M = 0.9)

$\left(\Delta C_{D_o}\right)_M$ zero lift drag-rise coefficient due to wing modification, taken as difference in ΔC_{D_o} between modified and unmodified models

C_L lift coefficient, $\frac{\text{lift}}{qS}$

C_m pitching-moment coefficient about the quarter-chord point of the mean aerodynamic chord, $\frac{\text{pitching moment}}{qS\bar{c}}$

$\left(\frac{L}{D}\right)_{max}$ maximum ratio of lift to drag

M free-stream Mach number

R Reynolds number, based on $\bar{c}$ of basic wing

S wing area, sq ft

V free-stream velocity, ft/sec

b wing span, ft

c local wing chord of basic wing, measured parallel to the model center line, ft

c' local chord of NACA 64A006 section of basic wing, ft

$\bar{c}$ mean aerodynamic chord, measured parallel to the model center line, $\frac{\int_o^{b/2} c^2 dy}{\int_o^{b/2} c\, dy}$

c_l section lift coefficient, $\frac{\text{section lift}}{qc}$

c_{l_i} section design lift coefficient

q free-stream dynamic pressure, $\frac{1}{2}\rho V^2$, lb/sq ft

y lateral coordinate perpendicular to the plane of symmetry, ft

α angle of attack, referred to body axis, deg

ϵ efficiency factor, ratio of effective aspect ratio to true aspect ratio

δ_f flap deflection measured perpendicular to hinge line, deg

ρ air density, slugs/cu ft

Subscripts

max maximum

u uncorrected

MODELS AND APPARATUS

Model for Low-Speed Large-Scale Tests

The model consisted of a wing and body, with a vertical tail installed for some of the tests. Figure 1 presents a two-view drawing with pertinent dimensions, and also illustrates the airfoil section modification used. Geometric data for the model are tabulated in table I. The model was tested in the Ames 40- by 80-foot wind tunnel and was supported on a conventional three-strut support system.

The fuselage and vertical tail are described in reference 4. The basic wing had an aspect ratio of 3, taper ratio of 0.4, leading-edge sweep of 45°, and an NACA 64A006 airfoil section perpendicular to its own quarter-chord line, which was swept 39.45°. The modified airfoil section was applied perpendicular to the same sweep line. The derivation of the modified section is given in Appendix A. Coordinates of the NACA 64A006 airfoil section and of the modified airfoil section are given in table II.

In addition to testing the model with the modified airfoil section incorporated over the full extent of the span, tests were made with the modification extending over the outboard 60 percent of the span only. For this case, the juncture between basic and modified portions of the wing was in a streamwise direction, and the model was tested both with a sharp and a faired discontinuity at the juncture. The fairing consisted of a piece of soft aluminum sheet wrapped around the leading edge. It extended about 5-percent semispan along the leading edge, and 40-percent chord on the lower surface.[1]

Split flaps were tested, at a 40° deflection only, on the modified model. The deflection was measured normal to the hinge line. The streamwise chord of the flaps was 25 percent of the local streamwise chord of the basic wing. The ends of each flap were cut perpendicular to the hinge line and the outboard end of the trailing edge, when the flap was undeflected, was located at 55 percent of the wing semispan.

[1]The term "modified model" will be understood hereinafter to refer to the model with full-span modification, whereas the model with partial-span modification will be termed the "partially modified model."

Model for High-Speed Tests

The model was tested in the Ames 6- by 6-foot supersonic wind tunnel. This tunnel has a closed section and is of the variable-pressure type. Its Mach number ranges are 0.6 to 0.9 and 1.2 to 1.9 (see ref. 5). In this tunnel models are sting-mounted with an internal electrical strain-gage balance.

The model consisted of a wing and body. Figure 2 presents a plan-view drawing of the model and pertinent dimensions. Geometric data are given in table I. The wing geometry was similar to that for the large-scale model. Airfoil section ordinates for both basic and modified sections are tabulated in table II.

The body used was geometrically similar to the body used in the low-speed tests. It was truncated, however, to accommodate the internal balance.

TESTS AND CORRECTIONS

Low-Speed Large-Scale Tests

Force and moment data were obtained at angles of attack from -2° to $+24^{\circ}$. The dynamic pressure for most of the tests was 25 pounds per square foot. The corresponding Reynolds number was 9.7×10^{6}, and the corresponding Mach number was 0.13. Some of the tests were made at Reynolds numbers from 4.4×10^{6} to 21×10^{6}, the corresponding dynamic pressures varying from 5.7 to 129 pounds per square foot, and the corresponding Mach numbers varying from 0.06 to 0.31. All data were corrected for air-stream inclination, wind-tunnel-wall effects, and support-strut interference.

High-Speed Tests

Force and moment data were obtained at angles of attack varying from -4° to a maximum of $+17^{\circ}$ at Mach numbers from 0.60 to 0.90 and from 1.20 to 1.90. Data were obtained at a Reynolds number of 2.9×10^{6} at all Mach numbers and at additional Reynolds numbers of 3.8 and 5.7×10^{6} at high subsonic speeds.

These data have been corrected for the following factors: (1) constriction of the air stream by the walls of the wind tunnel at subsonic speeds, (2) wind-tunnel-wall induced effects at subsonic speeds, (3) inclination of the air stream, (4) effect on the drag measurements due to the longitudinal variation of static pressure in the test section, and (5) the effect of support interference on the drag measurements. For the latter correction the base pressure was measured and the drag data adjusted to correspond to a base pressure equal to the static pressure of the free stream.

Reduction of Data

All angles of attack are referred to the chord plane of the basic wing. Unless otherwise noted, all force and moment coefficients are based on the area and mean aerodynamic chord of the basic wing. All pitching moments are computed about the quarter-chord point of the mean aerodynamic chord of the basic wing.

RESULTS AND DISCUSSION

Low-Speed Characteristics at $R = 9.7 \times 10^6$

The force data indicate that incorporation of the airfoil section modification along the entire wing span of the model resulted in the maintenance of attached flow over the wing at lift coefficients up to 0.92, with very little flow separation up to a C_L of 1.05. By contrast, flow separation on the basic wing, as indicated by the force data, occurred at a C_L of 0.39, spreading rapidly at lift coefficients above 0.6.

The force data upon which these conclusions are based are presented in figure 3. The fundamental improvement due to the modification is best indicated by the drag polars of figure 3(b), in which the range of parabolic drag variation is shown. Flow-separation effects on the longitudinal stability and high-lift characteristics of the two models can be seen in figure 3(a), in which longitudinal instability is indicated at $C_L = 0.61$ for the basic model and at $C_L = 1.05$ for the modified model.

Results for the modified model with split flaps are presented in figure 4. As the drag polar indicates, attached flow was maintained up to $C_L = 1.04$, with very little flow separation up to $C_{L_{max}}$ (1.17). Longitudinal instability does not occur until $C_{L_{max}}$.

The partial-span modification of the wing was tested because span-loading analysis indicated that the stability benefits of the full-span modification might be retained in spite of an expected earlier drag break. (See Appendix B for detailed discussion.) The results are presented in figure 5, with the curves for the fully modified model included for comparison. As the figure shows, removal of the modification from the 40-percent-semispan station inboard, with or without a smooth fairing of the discontinuity, resulted in flow separation at lower lift coefficients, as expected. The drag breaks occurred at or below $C_L = 0.55$, and longitudinal instability occurred at $C_L = 0.95$ for the abrupt-discontinuity configuration, and at $C_L = 0.85$ for the faired-discontinuity configuration. It can be seen that the partial modification still gave very significant improvement in stability and drag over the characteristics of the basic model.

Predictions based on two-dimensional data have been made of the low-speed effects of the full-span and partial-span modifications of the wing. These are developed in detail and compared with the measured characteristics in Appendix B.

High-Speed Characteristics at $R = 2.9 \times 10^6$

Effect of the modification on the longitudinal stability.- The reduction in longitudinal stability of the basic model at lift coefficients of about 0.6, which manifests itself as instability at low speed, was alleviated by increasing Mach number (fig. 6(b)). As a result, no marked improvement of the pitching-moment characteristics at high speeds was anticipated to result from the modification. The modification did result, however, in a negative increment of pitching-moment coefficient at zero lift. As a consequence, some increase in trim drag must be expected for an airplane configuration employing the modified wing.

Effect of the modification on C_{D_o}.- Perhaps the most important high-speed effect of the full-span modification is the increment of C_{D_o} to which it gives rise, especially at supersonic speeds. This increment is evident in figure 6(c), which presents the high-speed drag polars, and is brought out more clearly in figure 7, which is a cross plot of drag coefficient against Mach number at various lift coefficients. The increment in C_{D_o} at supersonic speeds varied from 0.0040 at a Mach number of 1.2 to 0.0075 at 1.9 (fig. 8). The sources of this increment, and the possibility of reducing or eliminating it through further modifications will be examined briefly.

The so-called "area rule" of linearized supersonic theory suggests that a part of the increment may have been caused by the change of area distribution associated with the increase of leading-edge radius. Therefore, calculations were made of the wave drag due to area distribution for each model at Mach numbers of 1.00 and 1.28 by the method of reference 6. (The computation was for the configuration with a closed body, corrected by subtracting the incremental difference between computed values for the closed body alone and for the foredrag of the truncated body alone.) The computed values are shown in figure 8, together with the measured transonic rise in C_{D_o} for both models.

The theoretical effect of the modification as such on the wave drag due to area distribution may be taken as the difference between the computed values for the two models. This difference is shown in figure 9, together with the difference in measured transonic drag rise between the two models.

The introduction of camber in the wing doubtless contributed to the wave drag of the modified model. However, it would be improper to conclude from figure 9 that the difference between theoretical and experimental values shown there provides a measure of that contribution. Because of the limitations of the method of reference 6, as discussed therein, the computed value of wave drag due to change of area distribution can only be taken as an order-of-magnitude indication. The only conclusion which should be drawn from figure 9 is that the change of area distribution associated with the increase of leading-edge radius gave rise to a significant part of the difference in drag rise between the models.

This conclusion implies that it should be possible to reduce appreciably the drag of the modified model at a particular design Mach number by adjusting the area distribution. Such adjustments could be made along the body or on the wing itself aft of 20-percent chord, without significant change in the low-speed characteristics of the model. Removal of the camber would provide further reduction in the wave drag with only a slight adverse change in the low-speed characteristics.

In addition to the wave-drag increments in C_{D_o} due to the modification, there was also an increase in C_{D_o} at subsonic speeds which presumably was due to a change in skin-friction drag. The theoretical two-dimensional pressure distributions for the wing sections indicate the occurrence of adverse pressure gradients much nearer the leading edge on both surfaces of the modified section, which would presumably result in much earlier boundary-layer transition. This earlier occurrence of adverse pressure gradients is due to the increased leading-edge radius and would not be materially affected by removal of the camber.

Effect of the modification on the drag at lifting conditions.- Subsonically the modification resulted in substantially less drag at the higher lift coefficients, as can be seen from figures 6 and 7. Supersonically, the increment of drag due to the modification decreased with increasing lift coefficient, resulting finally in an actual, though trivial, reduction in drag at the highest lift coefficients tested.

With regard to the effects to be expected from changes of area distribution, it would seem reasonable to assume that such changes along the body or over the rear portion of the wing should not materially affect the variation of drag with lift of either model. Therefore, if both models were modified to yield the same theoretical drag due to area distribution at a particular design Mach number, as suggested in the previous sections, the cross-over point of their polars at that Mach number would be expected to occur at a considerably lower lift coefficient than in the subject case.

The variation of $(L/D)_{max}$ with Mach number is presented in figure 10. At subsonic cruising speeds up to $M = 0.9$, the modification resulted in some improvement, while at supersonic speeds it resulted in some deterioration.

Effects of Reynolds Number at Subsonic Speeds

Because of the difference in Reynolds numbers between the low-speed and high-speed tests, further subsonic tests were run at different Reynolds numbers, both for the low-speed large-scale models and for the high-speed small-scale models. In the low-speed case, tests were run at Reynolds numbers from 4.4 to 21.1×10^6. (Reynolds number was varied by setting free-stream velocity, whence some of the effects may have been due to Mach number changes.) In the high-speed case, tests were run at Reynolds numbers from 2.9 to 5.7×10^6.

In general, it can be said that Reynolds number effects, in the ranges investigated, were minor. Figure 11 shows the low-speed variation of C_{D_o} with Reynolds number for both the basic and modified large-scale models. (For this figure only, drag coefficients for the modified model were based on true wing area, rather than on basic wing area. This reduced the values by 0.0002.) The figure indicates that Reynolds number had no appreciable effect on the difference in C_{D_o} between them. As in the high-subsonic-speed case, this difference was probably due in part to a more forward position of boundary-layer transition on both surfaces of the modified wing and, in this case, a further contribution may have arisen from the presence of lower surface irregularities on the modified wing due to the method of construction.[2]

Figures 12 and 13 present the low-speed longitudinal characteristics of the basic and modified models at Reynolds numbers from 4.4 to 20.6×10^6. For the modified model, fairing of the curves at high angles of attack is based on the data presented in figure 3. For this model, the lower initial peak of the lift curve at $R = 14.4 \times 10^6$, and the premature drag break at $R = 20.6 \times 10^6$ are probably due to attainment of critical velocities. At $M = 0.22$, corresponding to $R = 14.4 \times 10^6$, computation of critical pressure coefficients by equations of reference 7, using simple-sweep concepts, and based on unpublished pressure-distribution data for the model, indicates critical pressure coefficients may have been reached near a lift coefficient of 0.95. Similar computation at $M = 0.31$, corresponding to $R = 20.6 \times 10^6$, indicates critical pressure coefficients were probably

[2]It may be noted that in figure 3(b) the value of C_{D_o} for the basic model is indicated as being more than the value for the modified model. This is due to the fact that tubing from pressure orifices in the basic model was run down the tail strut, part of the tubing being exposed to the air stream and giving rise to some drag. This tubing was not present in the test of the modified model.

reached at outboard stations at a lift coefficient of about 0.65, somewhat before the measured drag break.

Figures 14 and 15 show that at high subsonic speeds, the aerodynamic characteristics of the basic and modified models were not significantly affected by varying the Reynolds number from 2.9 to 5.7×10^6. Attention is directed, however, to figure 14(b), wherein two sets of data for $R = 5.7\times10^6$ are shown on the drag polars. The principal set of data (unflagged symbols) was obtained after a piece of the original wing had been cut out of each wing panel and replaced with wax. The flagged symbols represent data obtained prior to this alteration. As can be seen, a discrepancy exists between the two sets of data at lift coefficients above 0.2. (To avoid cluttering the figure, no flagged symbols are shown below $C_L = 0.2$, since the two sets of data are in substantial agreement in this region.) No explanation for this discrepancy is evident at this time.

In figure 14(c), the data for $R = 5.7\times10^6$ were also obtained with the altered wing.

CONCLUDING REMARKS

The full-span wing modification reported upon herein showed the following:

1. Very marked improvement in stability, drag, and high-lift characteristics at low speeds, due to the maintenance of attached flow to high lift coefficients.

2. Less drag at the higher lift coefficients at Mach numbers up to 0.9.

3. A high-speed drag penalty at low lift coefficients, especially serious at supersonic Mach numbers.

Theoretical considerations indicate a significant part of the drag penalty is traceable to the change of area distribution associated with the modification, and that the drag of the modified model could be appreciably reduced at a particular design Mach number by adjustments of the area distribution along the body or over the rear portion of the wing without significant change in the low-speed benefits arising from the increased leading-edge radius.

Ames Aeronautical Laboratory
National Advisory Committee for Aeronautics
Moffett Field, Calif., Apr. 11, 1955

APPENDIX A

DESIGN OF THE MODIFIED AIRFOIL SECTION AND TWO-DIMENSIONAL TESTS

It was desired to modify the NACA 64A006 section to obtain a low-speed $c_{l_{max}}$ of 1.3 at a Reynolds number of 6×10^6, comparable to what might be expected from the use of a leading-edge flap. (See refs. 8 and 9.) An analysis of published two-dimensional data on 6-percent-thick sections showed a definite relation between the leading-edge radius and the $c_{l_{max}}$. A plot of $c_{l_{max}}$ versus leading-edge radius for a series of 6-percent-thick symmetrical sections (data from refs. 8, 10, 11, and 12) is shown in figure 16. Since, as can be seen from the plot, a $c_{l_{max}}$ of only 1.2 could safely be expected at $R = 6\times10^6$ from the use of large leading-edge radius alone, the addition of a slight amount of camber would be required to attain a $c_{l_{max}}$ of 1.3. The assumption was made that the small increment of $c_{l_{max}}$ desired could be attained if the design lift coefficient of the desired section were made approximately equal to that increment.

The NACA 0006-92 airfoil section was chosen as the basis for the thickness distribution since the value of its leading-edge radius (1.19 percent chord) was in the optimum range. The NACA 0006-92 contour was superposed on the NACA 64A006 contour so as to fair in smoothly on the upper surface and to provide the approximate degree of camber desired. The contour of the lower surface was designed to fair in to the NACA 64A006 section at the latter's point of maximum thickness. The mean line adopted ahead of that point consisted of two regions, one being an arc parallel to the upper surface from the fairing-in point forward, and the other being a straight line from the leading edge tangent to that arc. The point of tangency occurred at about 20-percent chord. The resulting section, therefore, was of constant maximum thickness from approximately 20-percent chord to approximately 40-percent chord. It should be noted that the mean line was not intended to approximate any existing standard mean line. The final section ordinates are given in table II, and the section is illustrated in figure 1. (As shown in the table, the lower surface ordinates of the section used in the small-scale wing differed slightly from those used in the large-scale wing and in the two-dimensional model described below. The extent of the difference is thought to be aerodynamically insignificant.)

A computation of the section ideal lift coefficient by the methods of references 13 and 14 (using the NACA 0006-92 airfoil section as reference base profile) yielded a value of $c_{l_i} = 0.08$, whence a reasonable estimate of $c_{l_{max}}$ at $R = 6\times10^6$ would be of the order of 1.3.

A two-dimensional model of the final airfoil section was tested in a 2- by 5-foot open-circuit wind tunnel. The model had a 2-foot chord and completely spanned the 2-foot height of the wind tunnel. It was equipped with 55 pressure orifices at midspan. Tests were made at a dynamic pressure of 25 pounds per square foot which resulted in a Reynolds number of 2.0×10^6. Pressure-distribution data were obtained at the midspan of the model at angles of attack from -2° to $+11^\circ$. The variation of section lift coefficient with angle of attack was obtained by mechanical integration of the pressure distribution. Corrections were not applied to the data obtained.

The lift curve for the modified airfoil section, as determined from the pressure-distribution measurements, is presented in figure 17. The measured value of $c_{l_{max}}$ was 1.30. The pressure diagrams show that collapse of the leading-edge suction peak and loss of lift after $c_{l_{max}}$ occur simultaneously.

The two-dimensional lift curve for the NACA 64A006 airfoil section, obtained from reference 8, is presented in the same figure. The data were obtained at a Reynolds number of 5.8×10^6, and corrections were not applied. The measured value of $c_{l_{max}}$ was 0.89. The discontinuity in the lift curve at $c_l = 0.55$ occurred as a result of the collapse of the leading-edge suction peak.

The significance of the lift and pressure-distribution characteristics of the two airfoil sections as applied to the subject wing is discussed in Appendix B.

APPENDIX B

COMPARISON OF LOW-SPEED EXPERIMENTAL RESULTS WITH PREDICTED RESULTS

A comparison with prediction has been made of the drag and pitching-moment-coefficient breaks obtained for the various configurations of the low-speed tests. The method presented in reference 1 was used to make the predictions.

For the basic wing, the drag break was predicted to occur at $C_L = 0.28$. This three-dimensional C_L corresponds to the two-dimensional c_l at which the loss in leading-edge peak suction occurred. The decrease in stability, or pitching-moment break, was predicted to occur at $C_L = 0.45$, the three-dimensional C_L corresponding to the two-dimensional $c_{l_{max}}$.[1]

As pointed out in references 1 and 15, measured values of C_L for separation phenomena on a large number of sweptback wings were higher than predicted values. The predictions for the basic wing of this report are also conservative. The measured lift coefficient ($C_L = 0.39$) for the drag break is 39 percent above the predicted value. (It should be noted that the method of prediction gives no indication of whether the drag break will be serious.) The measured lift coefficient ($C_L = 0.61$) for the unstable pitching-moment break is 36 percent above the predicted value.

Reference 15 suggests the use of an empirical correction factor of 1.25 in making predictions for swept wings. This factor is based on an analysis of tests of a number of swept wings of aspect ratios 3.4 to 8. However, to indicate the usefulness of the method for predicting the effect of proposed modifications to a wing whose existing characteristics are known, a factor of 1.39, based on the drag results above, was used in predicting the characteristics of the modified configurations. A comparison of predictions and corresponding measurements is summarized in the following table:

[1]Since reference 1 dealt exclusively with airfoil sections for which maximum peak suction coincided with maximum section lift coefficient, all predictions therein were based on section maximum-lift-coefficient data exclusively.

Configuration	Drag break			Stability break		
	Uncorrected prediction	Corrected prediction	Measured value	Uncorrected prediction	Corrected prediction	Measured value
Basic model	0.28	----	0.39	0.45	----	0.61
Fully modified model	.65	0.91	.92	.65	0.91	1.05
Partially modified model, abrupt discontinuity of modification	.30	.42	.47	.65	.91	.95
Partially modified model, faired discontinuity of modification	.30	.42	.55	.65	.91	.85

For the partially modified configurations, the predicted drag break is based on the expectation of leading-edge separation at 40-percent semispan. Due to the proximity of the 40-percent semispan station to the center of pressure of the wing, complete section stall there would not be expected to produce any great change in stability over that measured at lower lift coefficients. Therefore, the stability break would be expected to result from section stall further outboard. Assuming that section stall at 40-percent semispan would not affect span loading outboard, the stability break can be predicted in the same manner as for the fully modified model, namely, at $C_L = 0.91$. While this prediction is considered in good agreement with measured values, a change of span loading is, nevertheless, evident from the fact that measured stability breaks for the two partially modified configurations differ both from that for the fully modified configuration and between themselves.

REFERENCES

1. Maki, Ralph L.: The Use of Two-Dimensional Section Data to Estimate the Low-Speed Wing Lift Coefficient at Which Section Stall First Appears on a Swept Wing. NACA RM A51E15, 1951.

2. Maki, Ralph L.: Full-Scale Wind-Tunnel Investigation of the Effects of Wing Modification and Horizontal-Tail Location on the Low-Speed Static Longitudinal Characteristics of a 35° Swept-Wing Airplane. NACA RM A52B05, 1952.

3. Demele, Fred A., and Sutton, Fred B.: The Effects of Increasing the Leading-Edge Radius and Adding Forward Camber on the Aerodynamic Characteristics of a Wing With 35° of Sweepback. NACA RM A50K28a, 1951.

4. Graham, David, and Koenig, David G.: Tests in the Ames 40- by 80-Foot Wind Tunnel of an Airplane Configuration With an Aspect Ratio 2 Triangular Wing and an All-Movable Horizontal Tail - Longitudinal Characteristics. NACA RM A51B21, 1951.

5. Frick, Charles W., and Olson, Robert N.: Flow Studies in the Asymmetric Adjustable Nozzle of the Ames 6- by 6-Foot Supersonic Wind Tunnel. NACA RM A9E24, 1949.

6. Holdaway, George H.: Comparison of Theoretical and Experimental Zero-Lift Drag-Rise Characteristics of Wing-Body-Tail Combinations Near the Speed of Sound. NACA RM A53H17, 1953.

7. von Karman, Theodor: Compressibility Effects in Aerodynamics. Jour. Aero. Sci., vol. 8, no. 9, July 1941, pp. 337-356.

8. McCullough, George B., and Gault, Donald E.: Boundary-Layer and Stalling Characteristics of the NACA 64A006 Airfoil Section. NACA TN 1923, 1949.

9. Nuber, Robert J., and Gottlief, Stanley M.: Two-Dimensional Wind-Tunnel Investigation at High Reynolds Numbers of an NACA 65A006 Airfoil With High-Lift Devices. NACA RM L7K06, 1948.

10. Abbott, Ira H., von Doenhoff, Albert E., and Stivers, Louis S., Jr.: Summary of Airfoil Data. NACA Rep. 824, 1945.

11. Loftin, Laurence K., Jr., and von Doenhoff, Albert E.: Exploratory Investigation at High and Low Subsonic Mach Numbers of Two Experimental 6-Percent-Thick Airfoil Sections Designed to Have High Maximum Lift Coefficients. NACA RM L51F06, 1951.

12. Paradiso, Nicholas J.: Investigation at High and Low Subsonic Mach Numbers of Two Symmetrical 6-Percent-Thick Airfoil Sections Designed to Have High Maximum Lift Coefficients at Low Speeds. NACA RM L52I02, 1952.

13. Allen, H. Julian: General Theory of Airfoil Sections Having Arbitrary Shape or Pressure Distribution. NACA Rep. 833, 1945.

14. Graham, David: A Modification to Thin-Airfoil-Section Theory, Applicable to Arbitrary Airfoil Sections, to Account for the Effects of Thickness on the Lift Distribution. NACA TN 2298, 1951.

15. Maki, Ralph L., and Embry, Ursel R.: Effects of High-Lift Devices and Horizontal-Tail Location on the Low-Speed Characteristics of a Large-Scale 45° Swept-Wing Airplane Configuration. NACA RM A54E10, 1954.

TABLE I.- GEOMETRIC DATA OF MODELS TESTED IN AMES 40- BY 80-FOOT AND 6- BY 6-FOOT WIND TUNNELS

	40- by 80-foot wind tunnel	6- by 6-foot supersonic wind tunnel
Basic wing		
Area	312.5 sq ft	350.0 sq in.
Span	30.62 ft	32.40 in.
Mean aerodynamic chord	10.83 ft	11.47 in.
Aspect ratio	3	3
Taper ratio	0.4	0.4
Leading-edge sweep, deg	45	45
Sweep of reference sweep line	39.45°	39.45°
Airfoil section, normal to reference sweep line	NACA 64A006	NACA 64A006
Modified wing		
Area	319.0 sq ft	357.1 sq in.
Span	30.62 ft	32.40 in.
Mean aerodynamic chord	11.05 ft	11.69 in.
Aspect ratio	2.94	2.94
Taper ratio	0.4	0.4
Leading-edge sweep, deg	45.33	45.33
Airfoil section, normal to reference sweep line	subject modification	subject modification
Incidence of true chord planes	-0.74°	-0.74°
Dihedral of true chord planes	-0.32°	-0.32°
Body		
Length	56.16 ft	46.93 in.
Length for closure	56.16 ft	59.50 in.
Maximum diameter	4.49 ft	4.76 in.
Fineness ratio, closed body	12.5	12.5
Vertical tail		
Exposed area	52.53 sq ft	
Aspect ratio	1	
Taper ratio	0	
Leading-edge sweep, deg	63.43	

TABLE II.- COORDINATES OF THE AIRFOIL SECTIONS USED

[All coordinates are referred to the chord of the NACA 64A006 section, and are in terms of percent of that chord. Asterisks indicate ordinates that are identical to those of the NACA 64A006 section.]

Station	NACA 64A006 ordinate	Ordinates of modified sections		
		Upper surface	Lower surface	
			Two-dimensional and large-scale models	High speed model
-1.50		-1.38	-1.38	-1.38
-1.25		-.60	-2.065	-2.065
-1.00		-.34	-2.315	-2.315
-.75		-.145	-2.49	-2.49
-.25		.16	-2.75	-2.75
0	0	.29	-2.855	-2.855
.25		.395	-2.955	-2.955
.50	.485	.49	-3.04	-3.04
.75	.585	*	-3.10	-3.10
1.25	.739		-3.22	-3.22
2.5	1.016		-3.405	-3.405
5.0	1.399		-3.60	-3.615
7.5	1.684		-3.67	-3.70
10	1.919		-3.68	-3.74
15	2.283		-3.61	-3.655
20	2.557		-3.45	-3.445
25	2.757		-3.235	-3.245
30	2.896		-3.095	-3.105
35	2.977		-3.02	-3.025
40	2.999		-3.000	-3.000
45	2.945		*	*
50	2.825			
55	2.653			
60	2.438			
65	2.188			
70	1.907			
75	1.602			
80	1.285			
85	.967			
90	.649			
95	.331			
100	.013			
Leading edge radius = 0.246		Leading-edge radius = 1.19 Center of leading-edge circle: x = -0.31 y = -1.33		
Maximum thickness of modified section in percent of true chord: 5.91 Maximum camber of modified section in percent of true chord: 0.90				

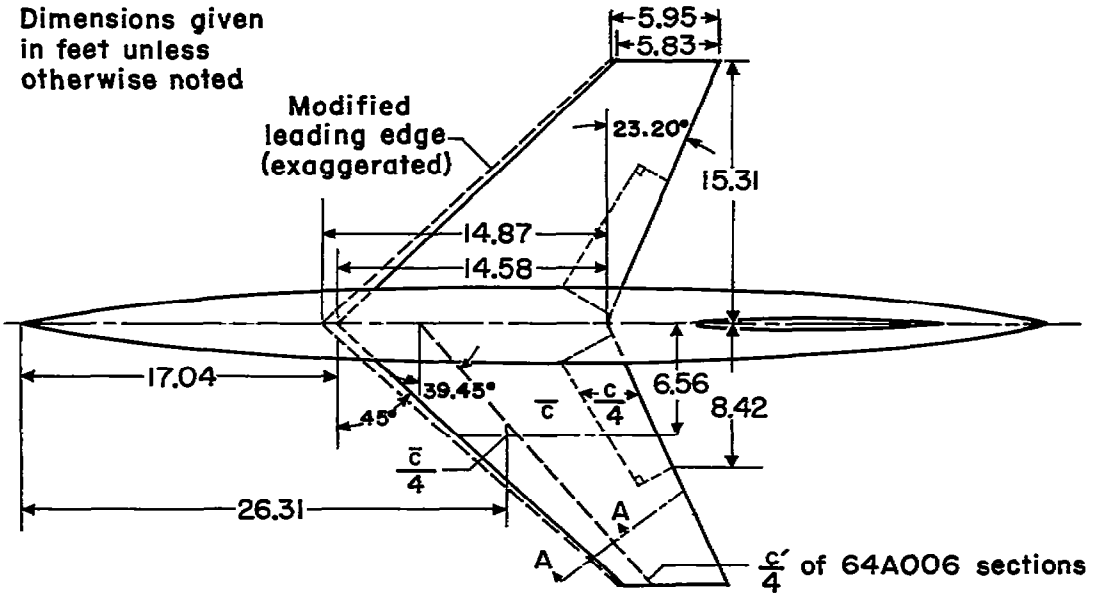

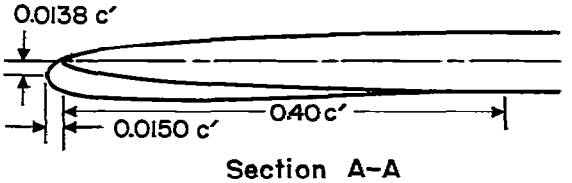

Section A-A
(used for two-dimensional model)

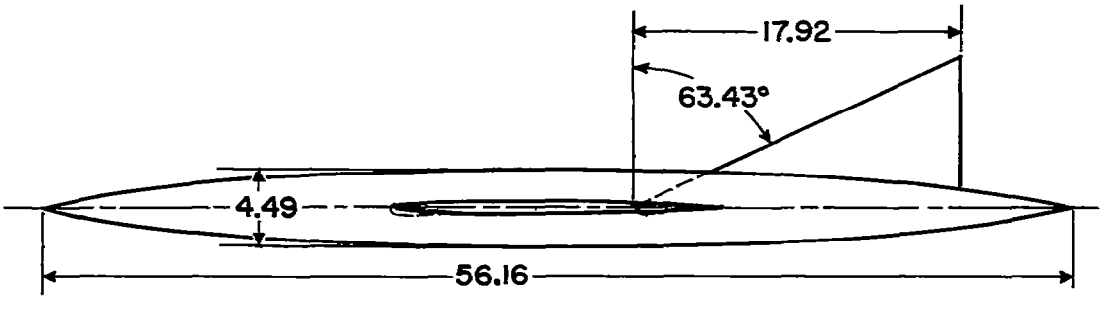

Figure 1.- Two-view drawing of the large-scale model tested at low speeds in the Ames 40- by 80-foot wind tunnel, and sketch of the modified wing section.

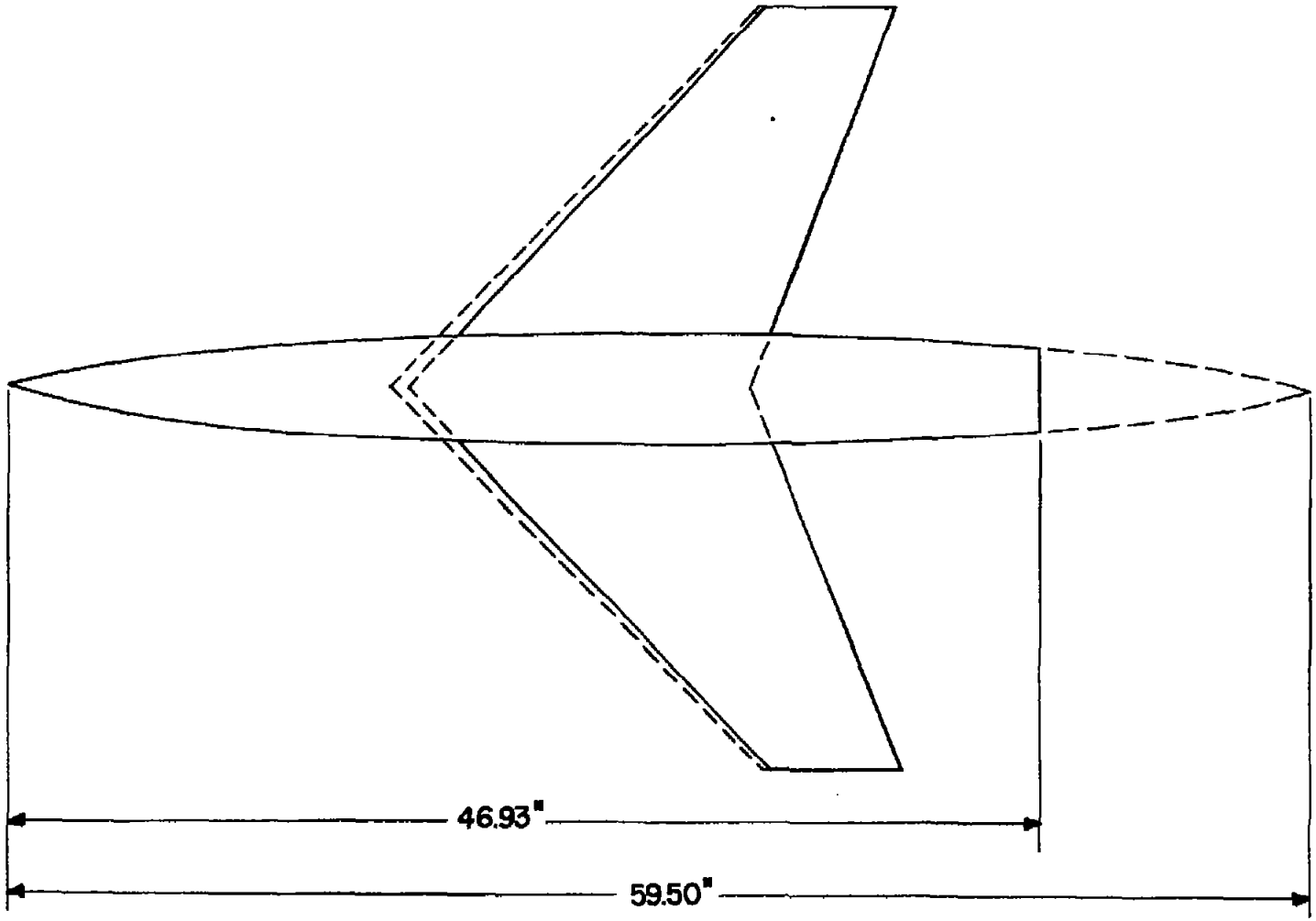

Figure 2.- Plan-view drawing of the small-scale model tested at high speeds in the Ames 6- by 6-foot supersonic wind tunnel.

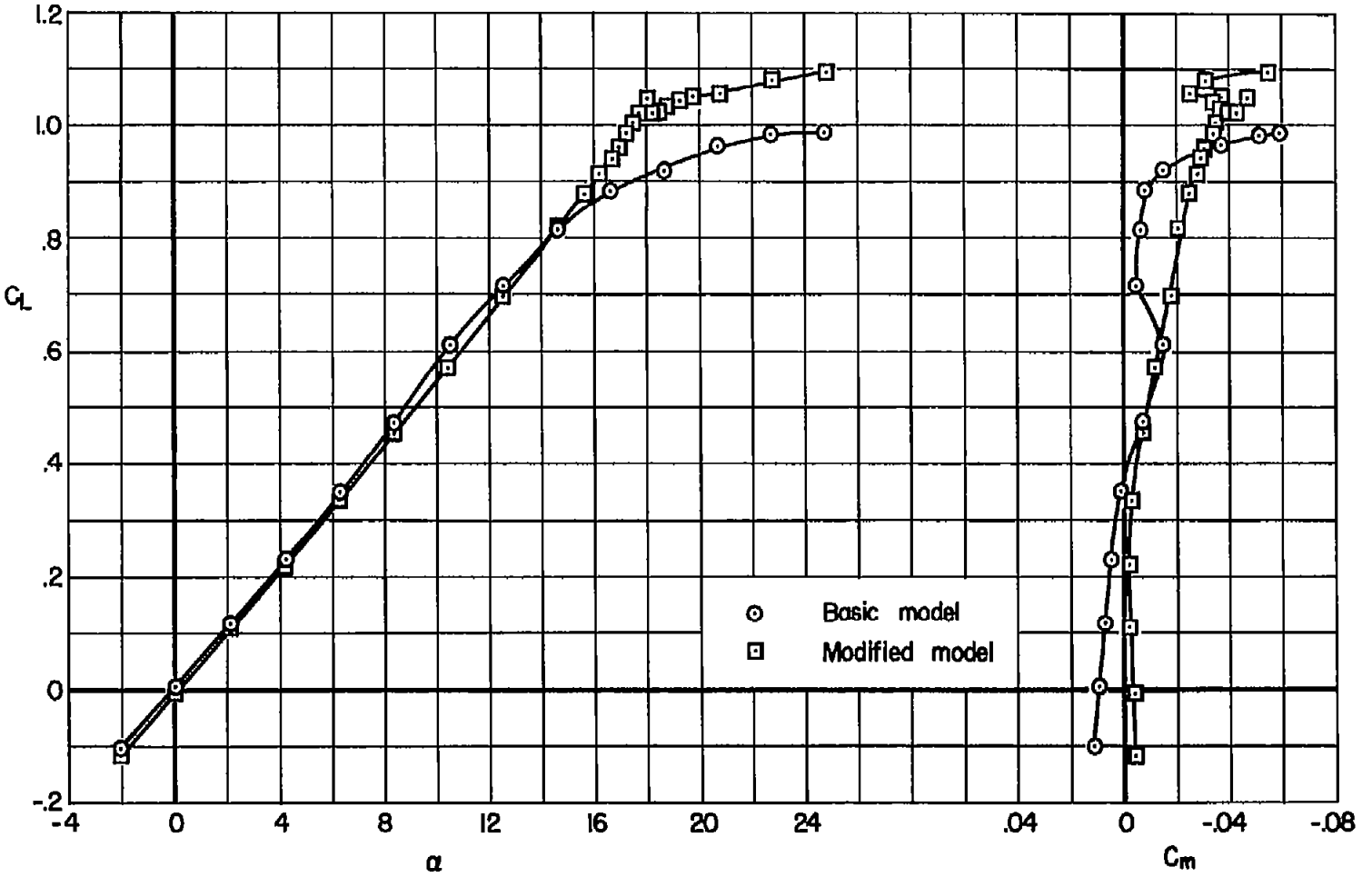

(a) C_L vs. α, C_m

Figure 3.- Low-speed aerodynamic characteristics of the basic and modified large-scale model with vertical tail installed; $R = 9.7 \times 10^6$.

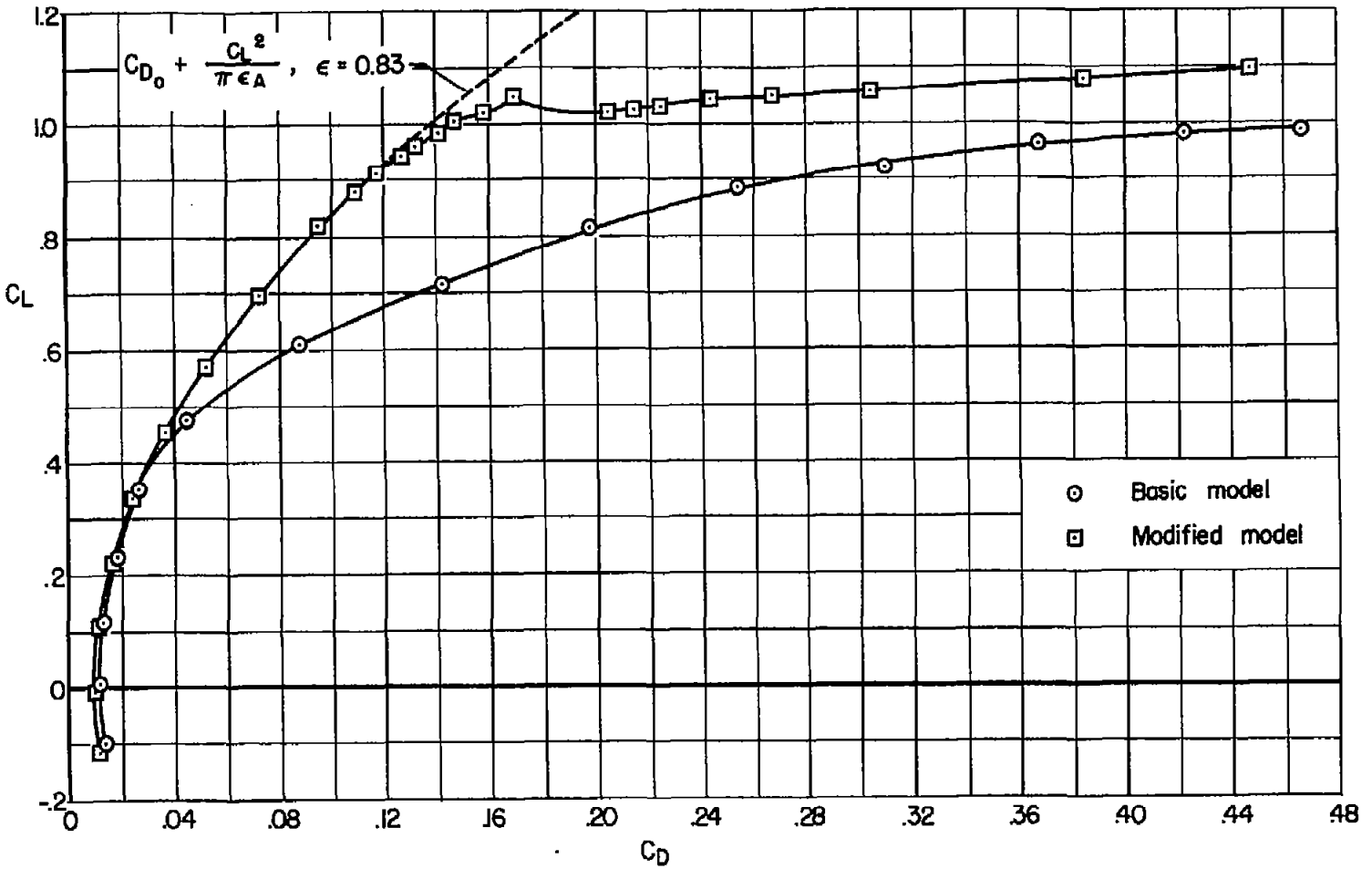

(b) C_L vs. C_D

Figure 3.- Concluded.

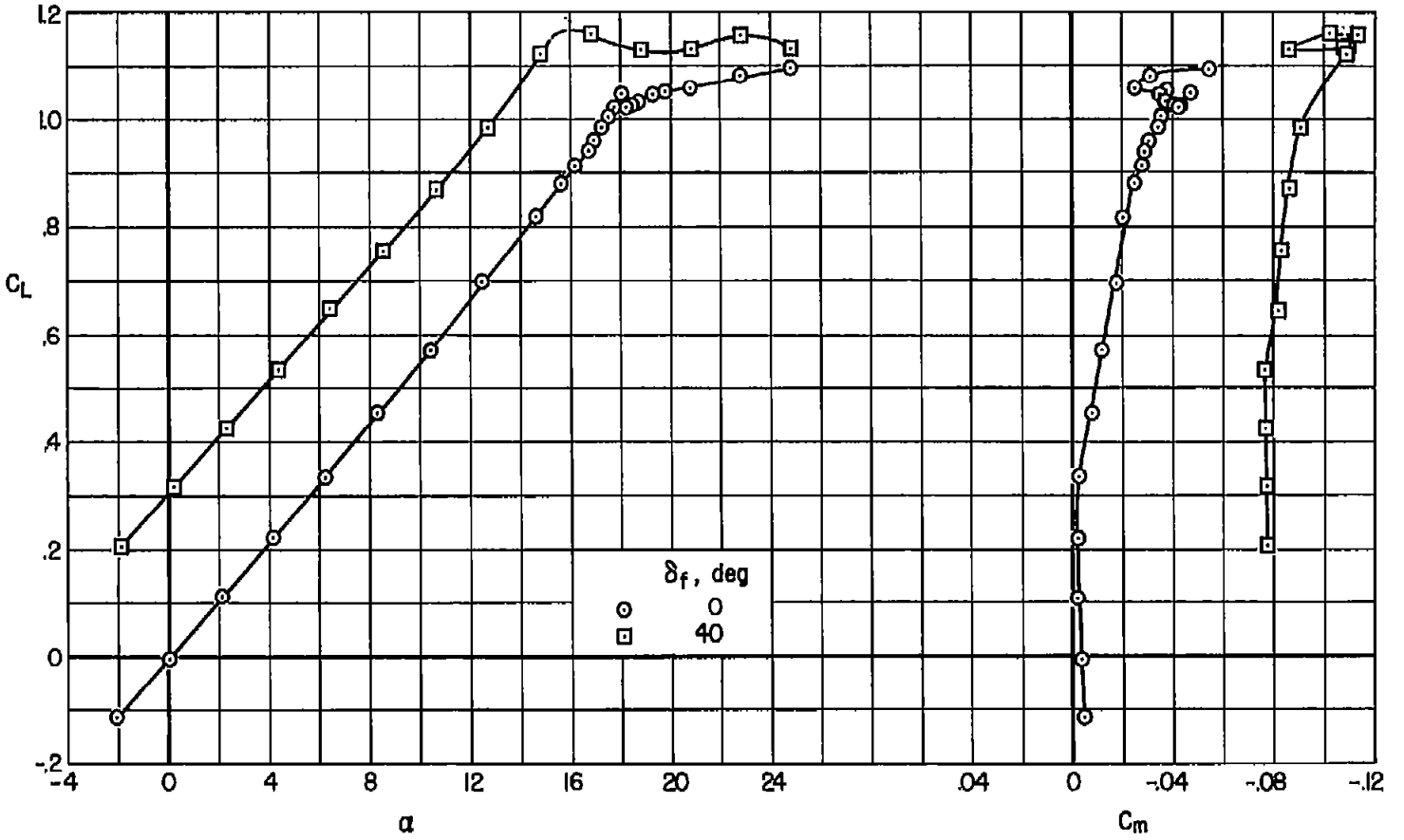

(a) C_L vs. α, C_m

Figure 4.- Low-speed aerodynamic characteristics of the modified large-scale model with split flaps, vertical tail installed; R = 9.7×10^6.

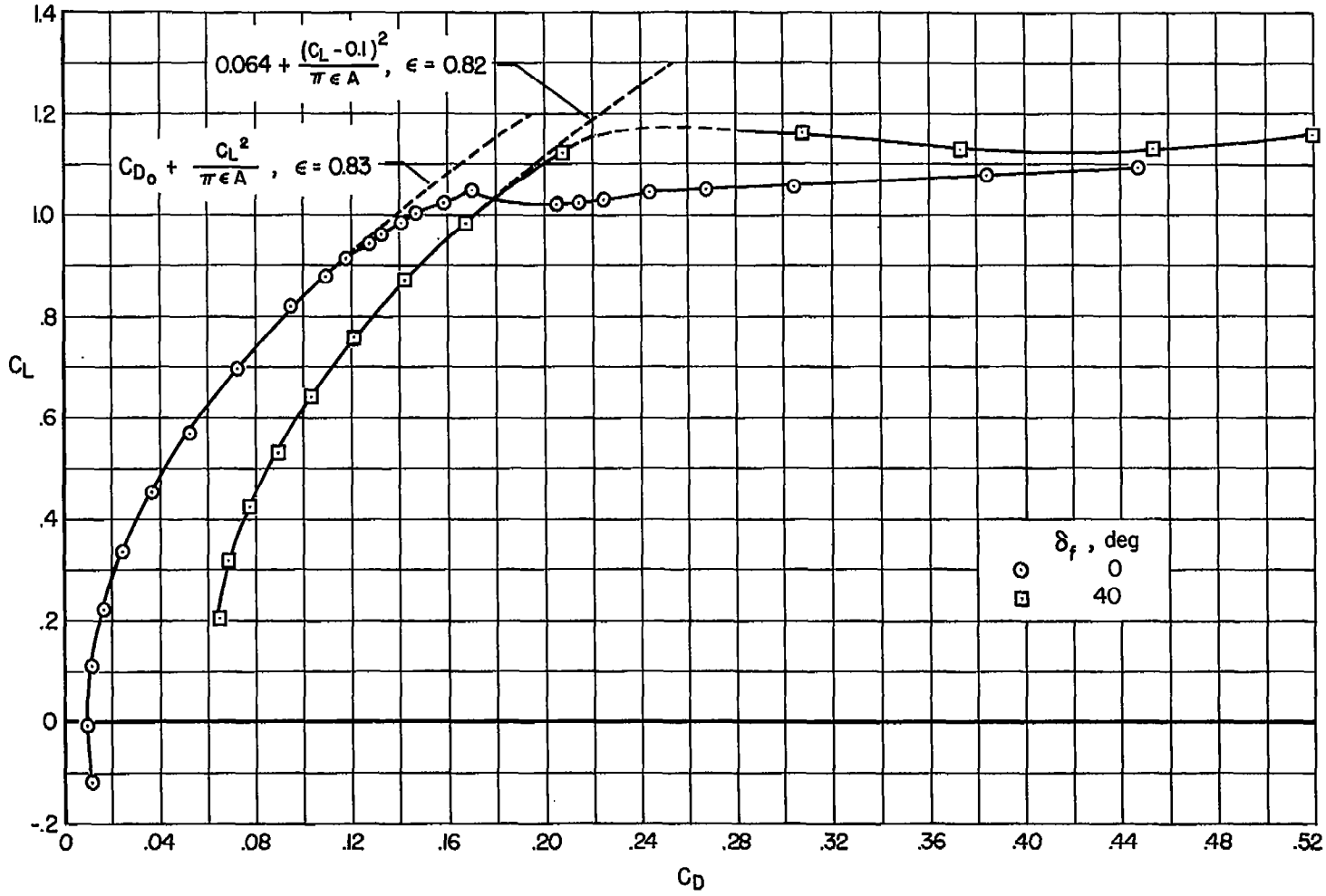

(b) C_L vs. C_D

Figure 4.- Concluded.

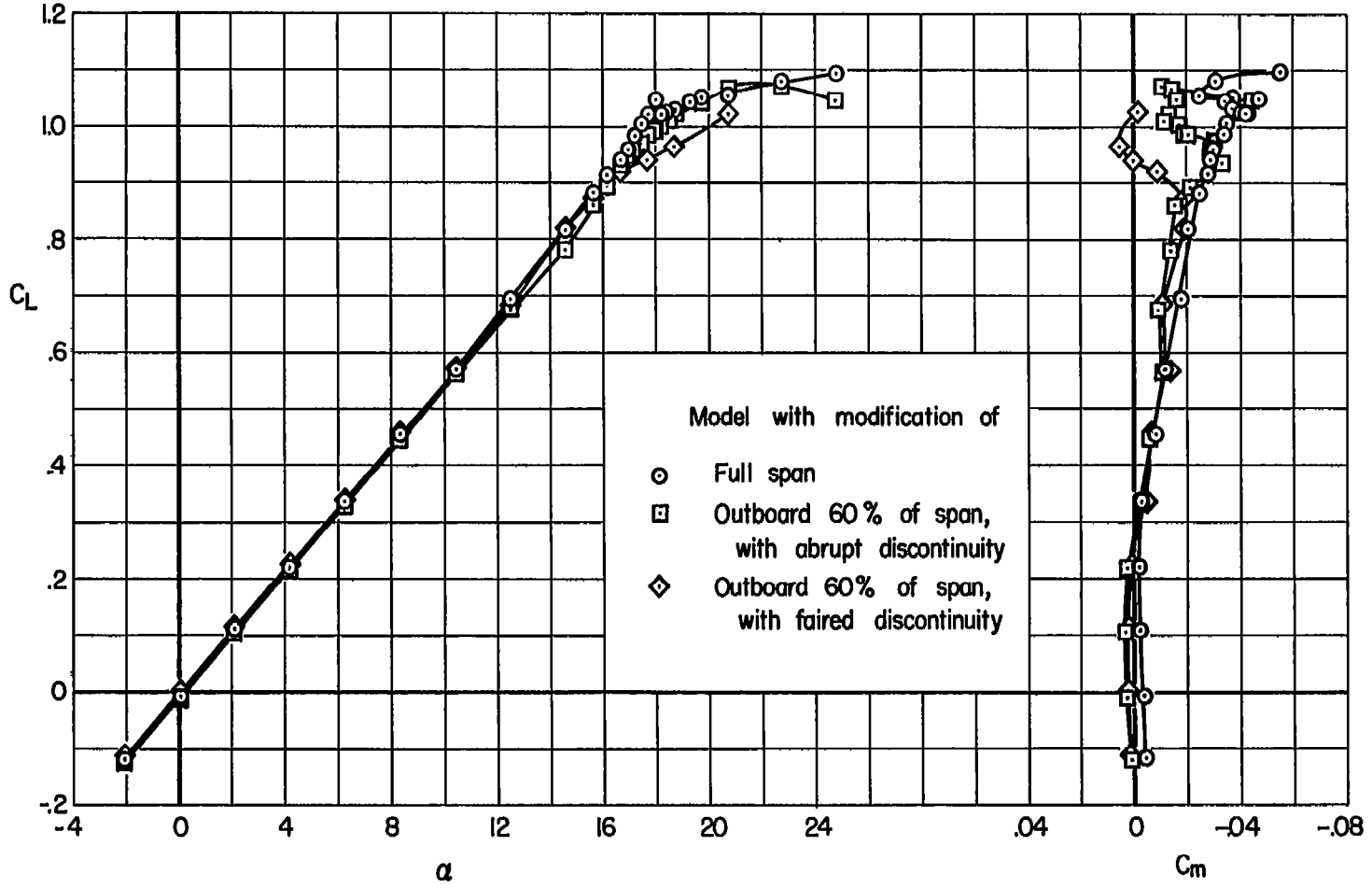

(a) C_L vs. α, C_m

Figure 5.- Low-speed aerodynamic characteristics of the fully modified and partially modified large-scale model, with vertical tail installed; R = 9.7×10^6.

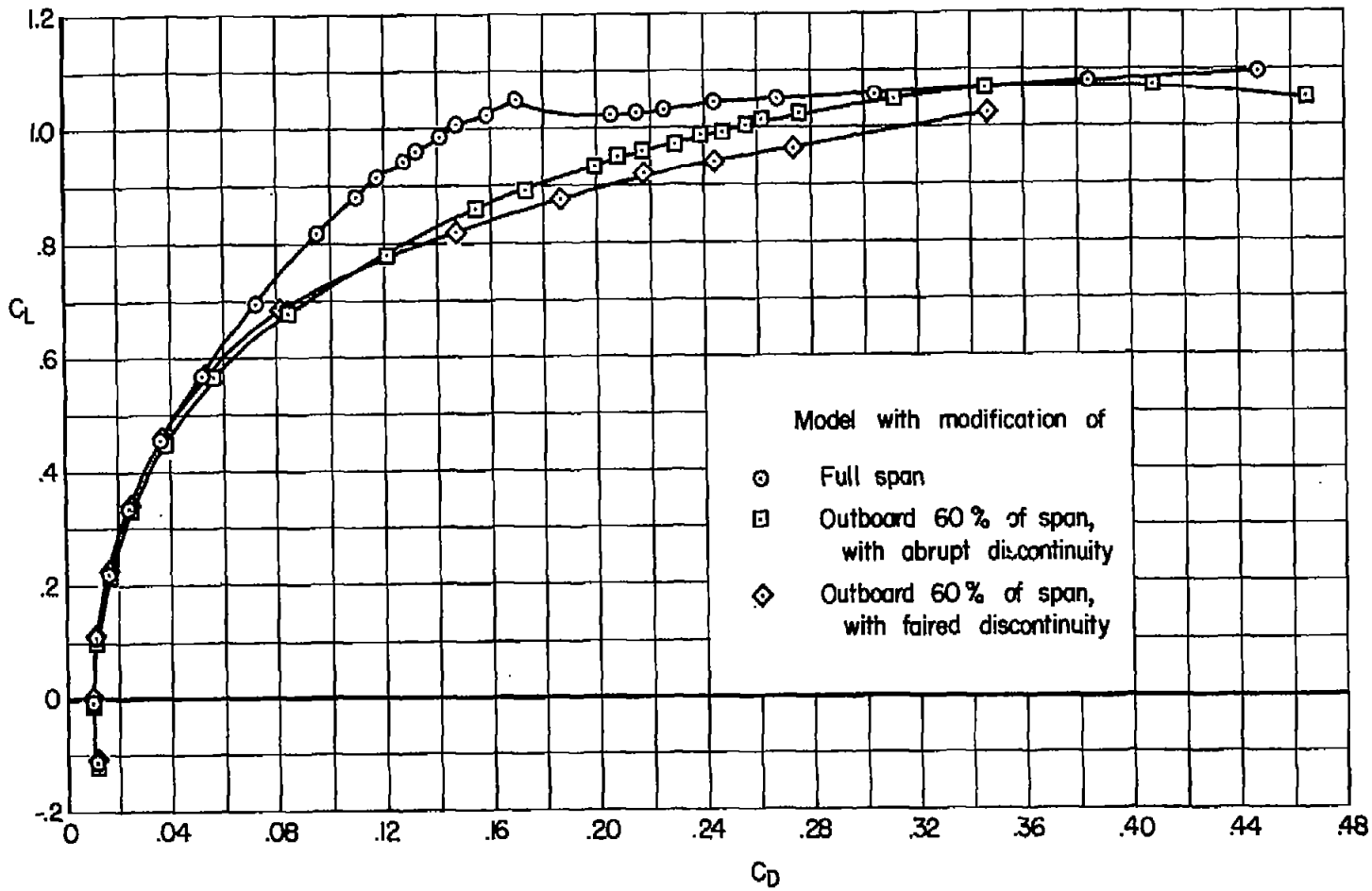

(b) C_L vs. C_D

Figure 5.- Concluded.

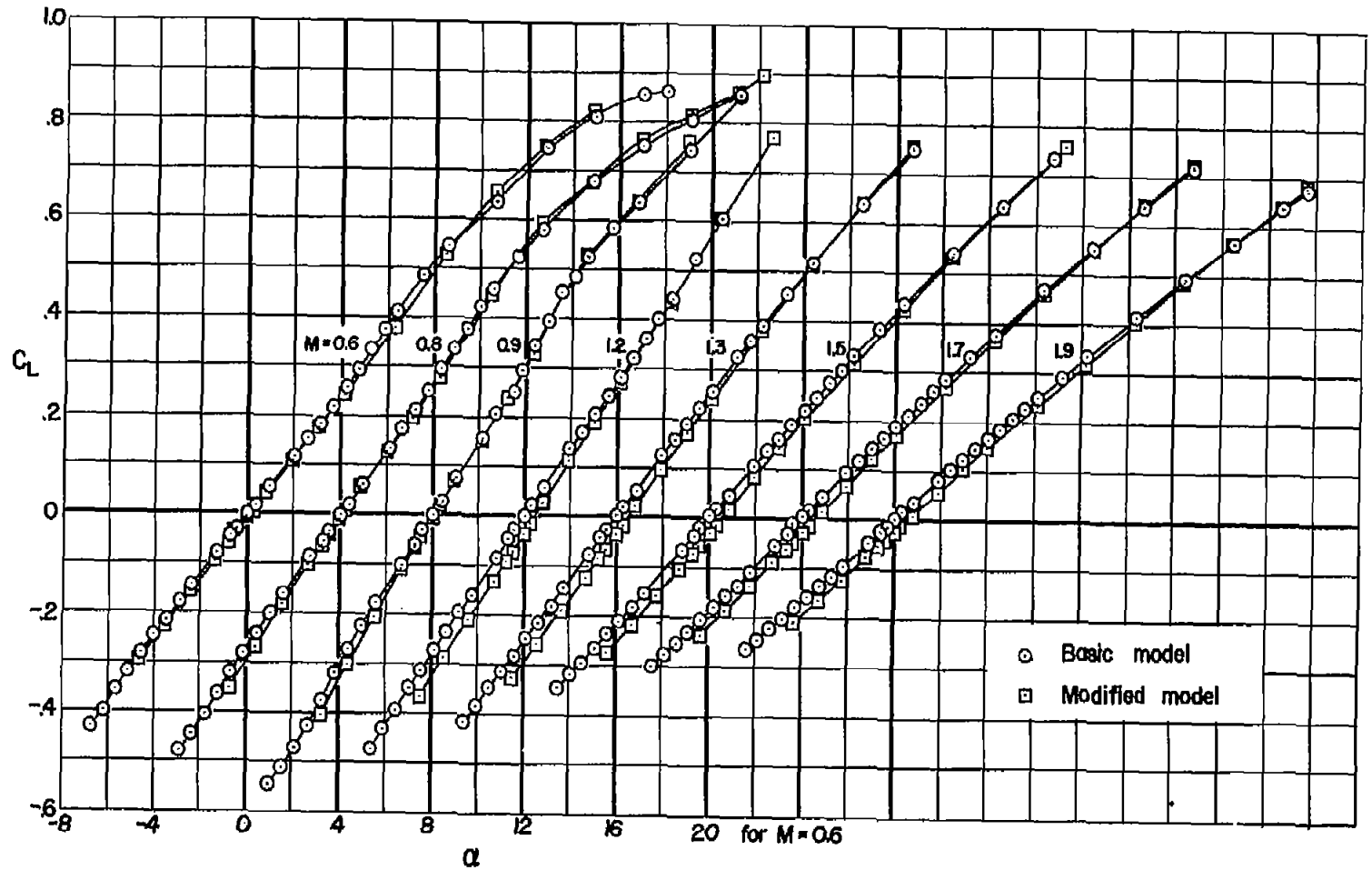

(a) C_L vs. α

Figure 6.- High-speed aerodynamic characteristics of the basic and modified small-scale model; $R = 2.9 \times 10^6$.

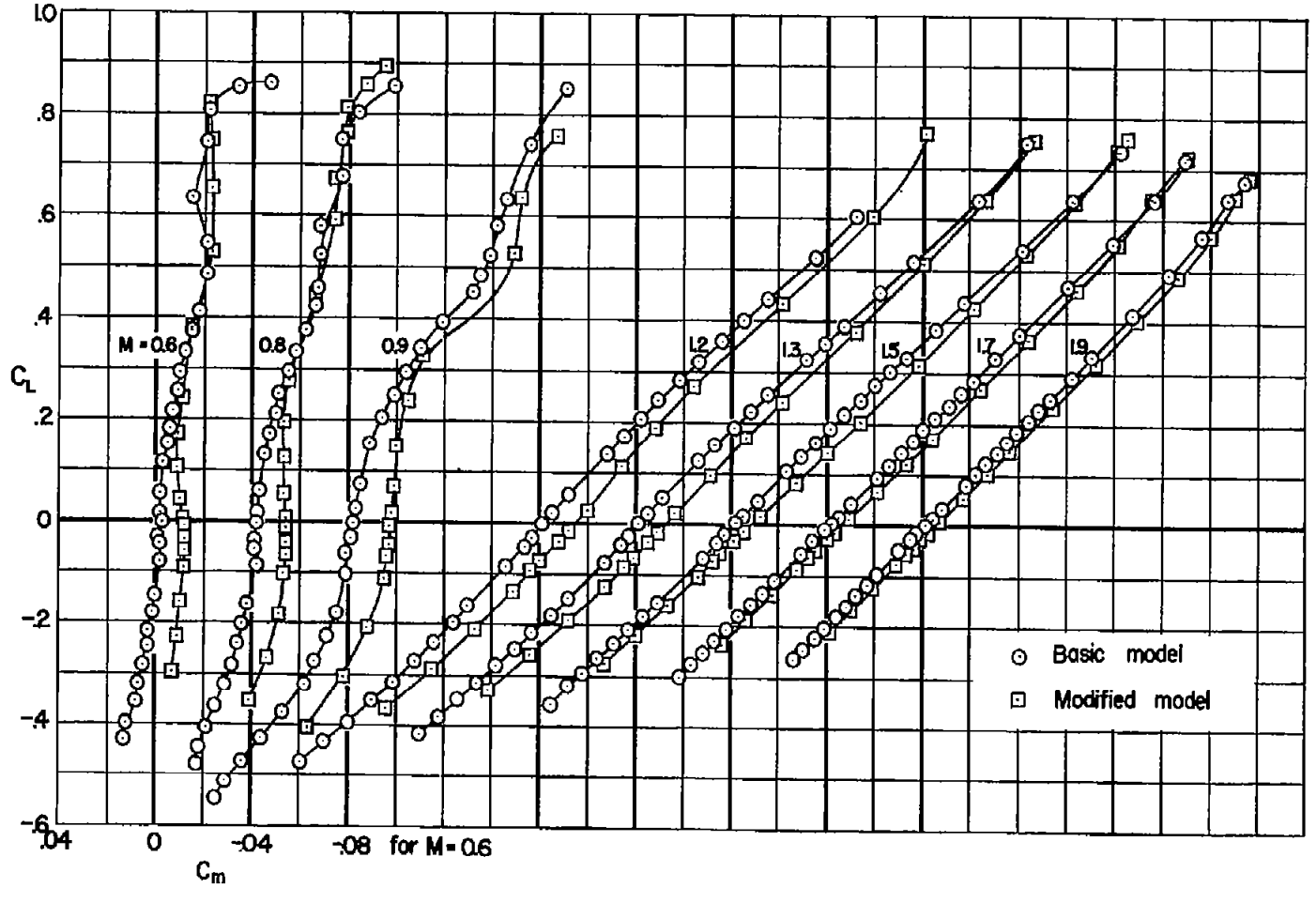

(b) C_L vs. C_m

Figure 6.- Continued.

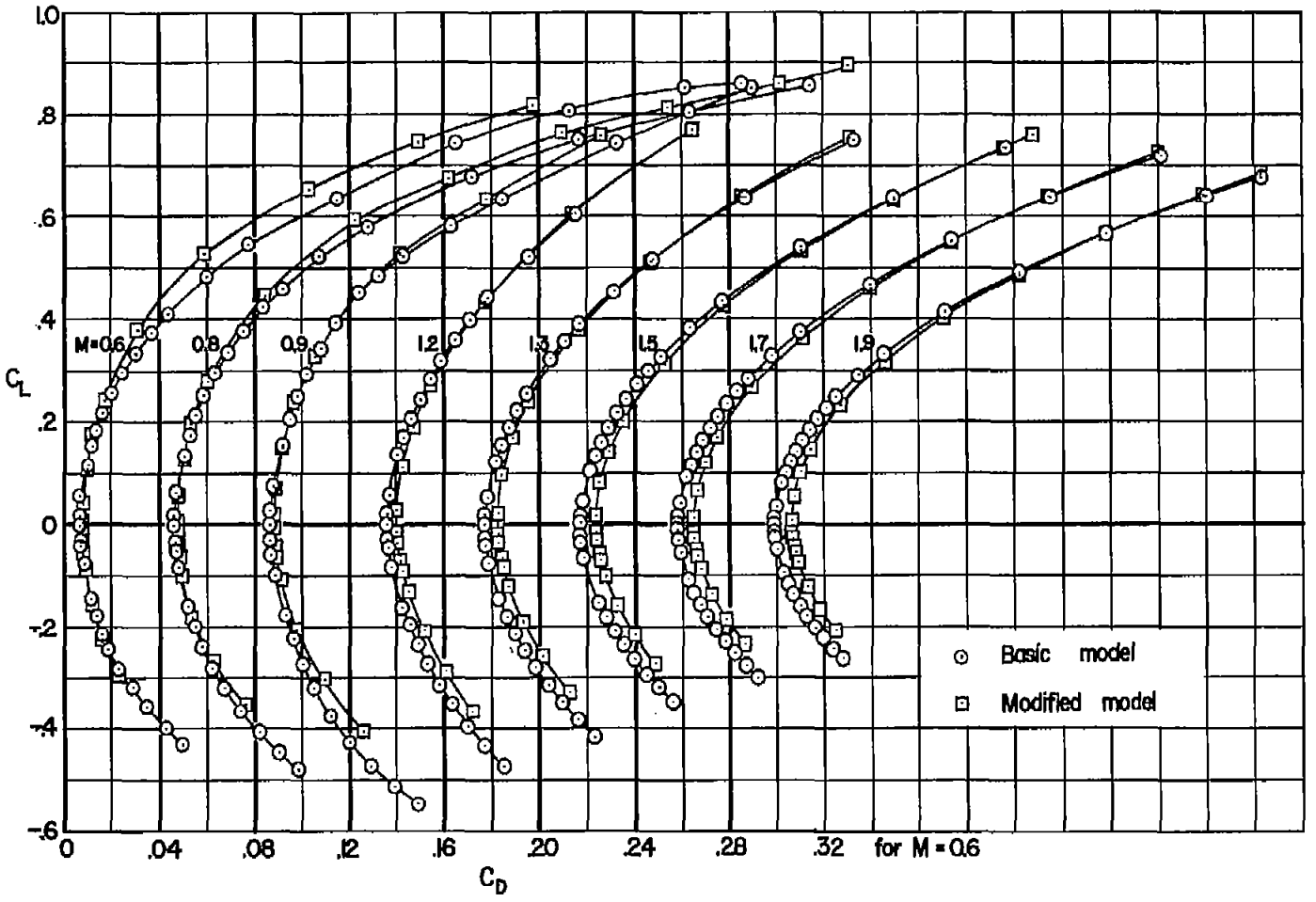

(c) C_L vs. C_D

Figure 6.- Concluded.

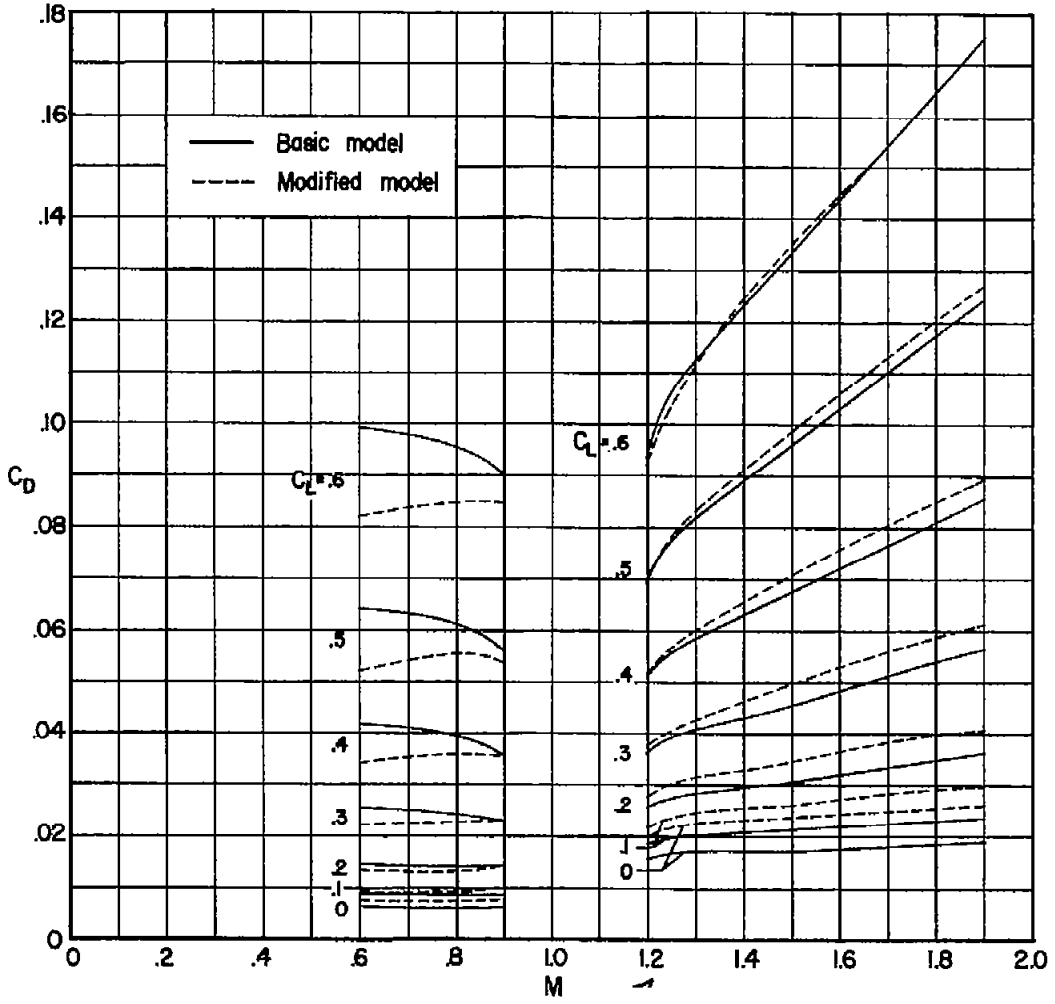

Figure 7.- Effect of Mach number on the drag coefficient of the basic and modified small-scale model at various lift coefficients; R = 2.9×10^6.

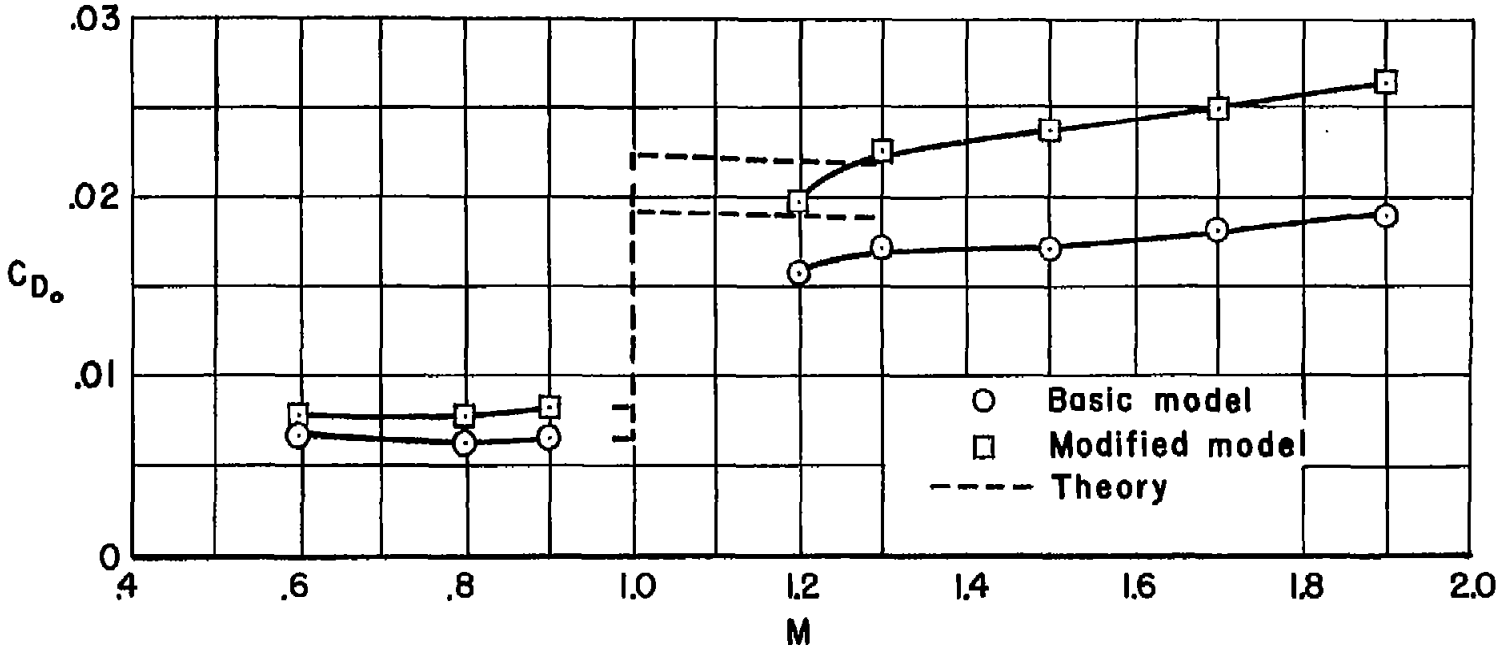

Figure 8.- Comparison of theoretical values of C_{D_o} for the wing-body combinations, camber being neglected, with measured values for the models at $R = 2.9 \times 10^6$.

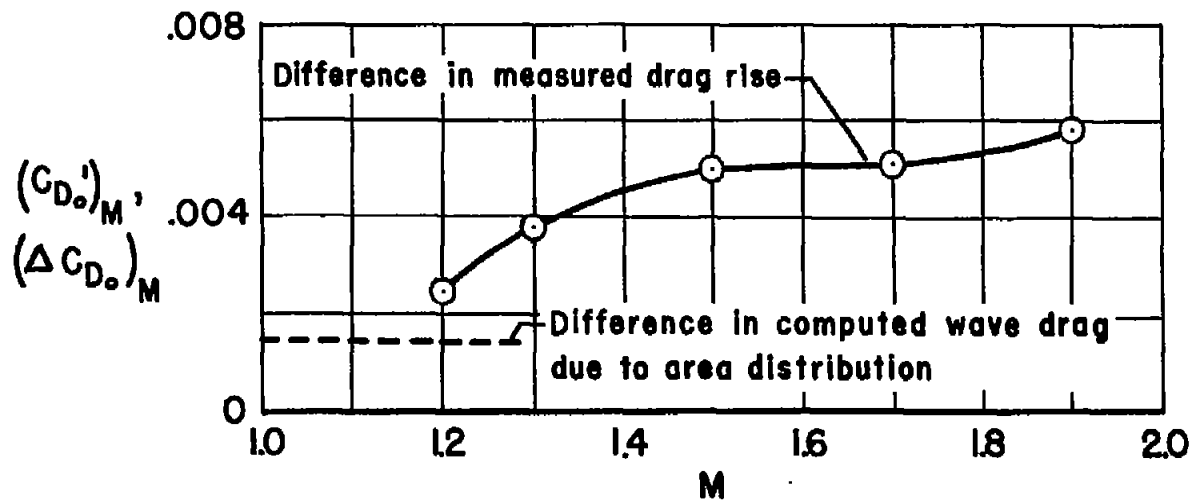

Figure 9.- Comparison of the difference in theoretical wave drag between the wing-body combinations with the difference in measured transonic drag rise between the models at $R = 2.9 \times 10^6$.

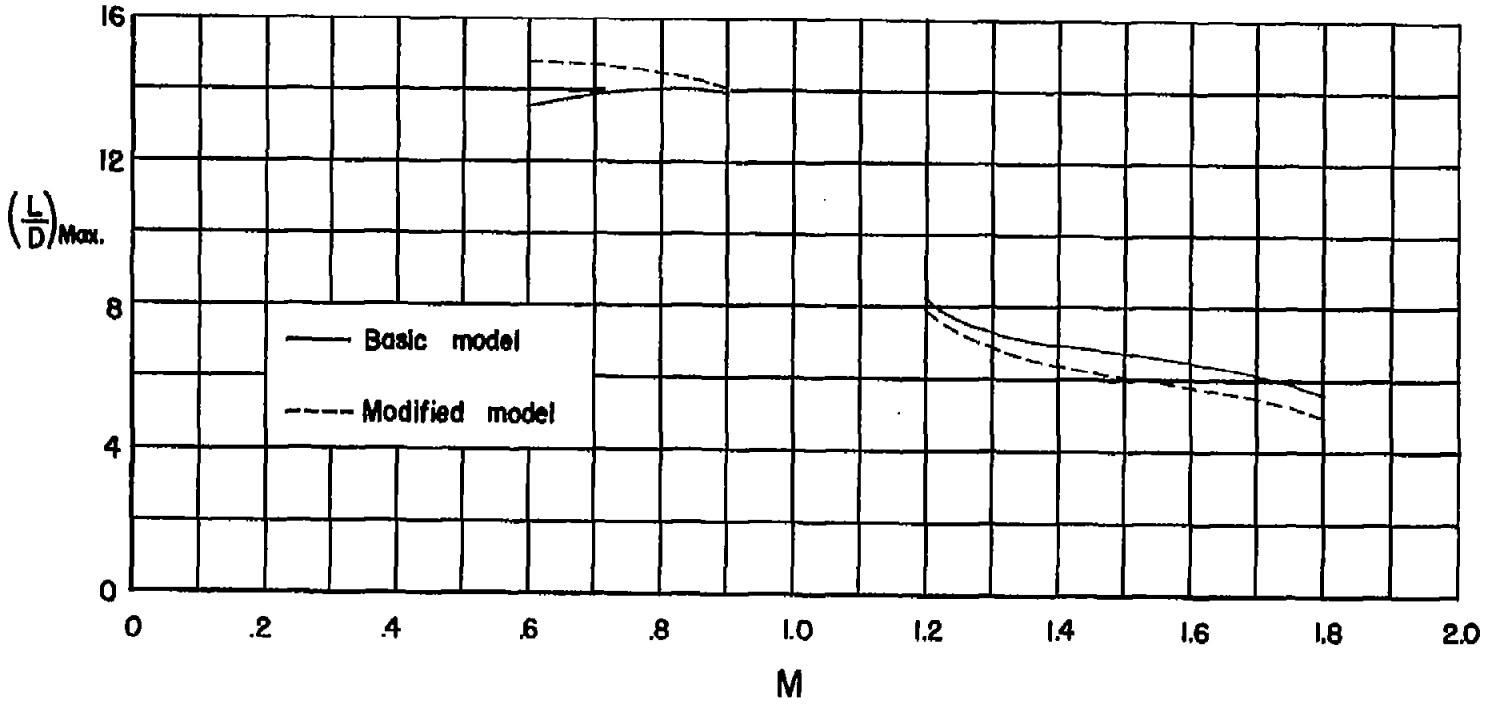

Figure 10.- Effect of Mach number on $(L/D)_{max}$ for the basic and modified small-scale model; $R = 2.9 \times 10^6$.

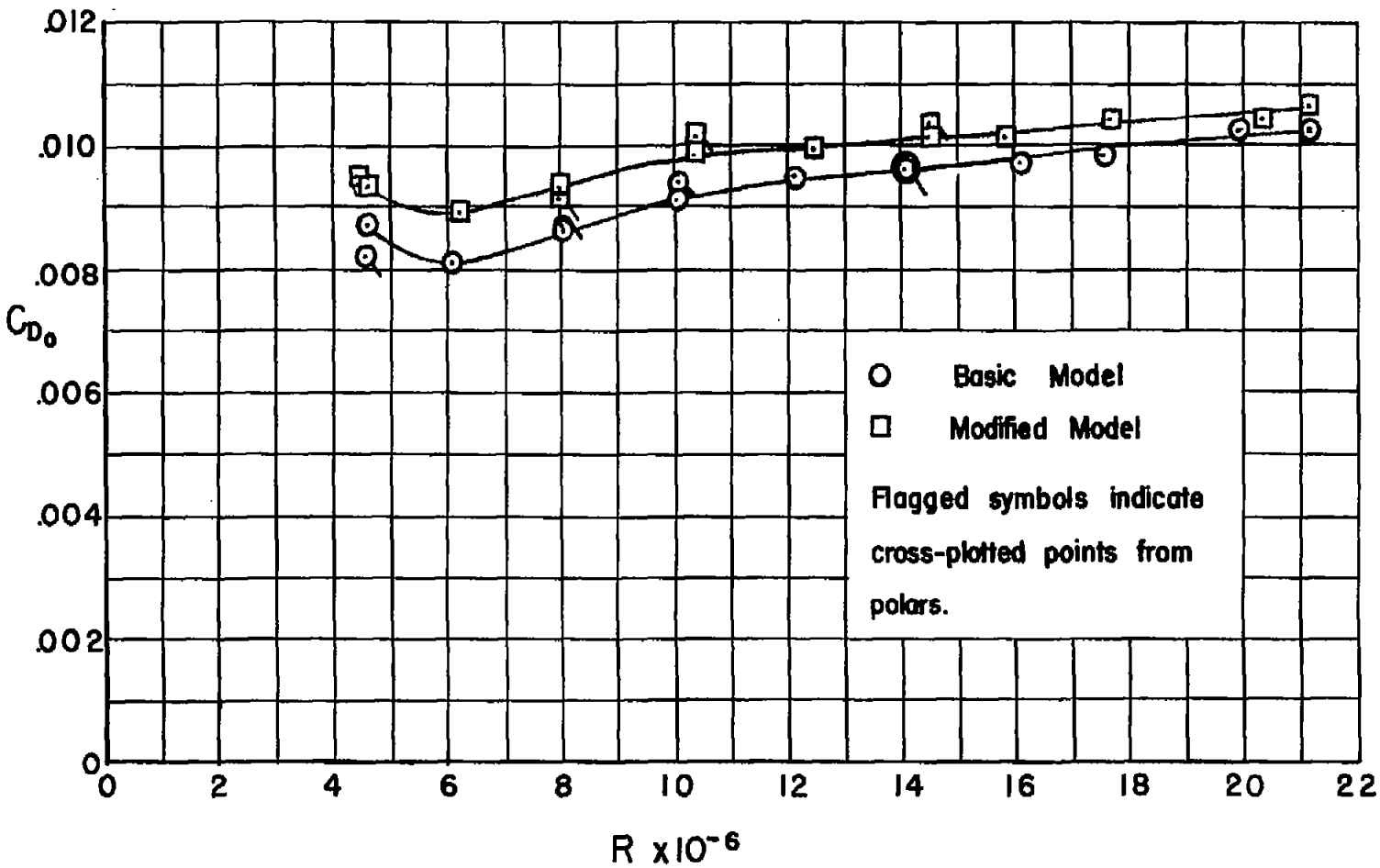

Figure 11.- Low-speed effect of Reynolds number on C_{D_o} for the basic and modified large-scale model, without the vertical tail. For the modified model, C_{D_o} is based on true wing area rather than modified wing area.

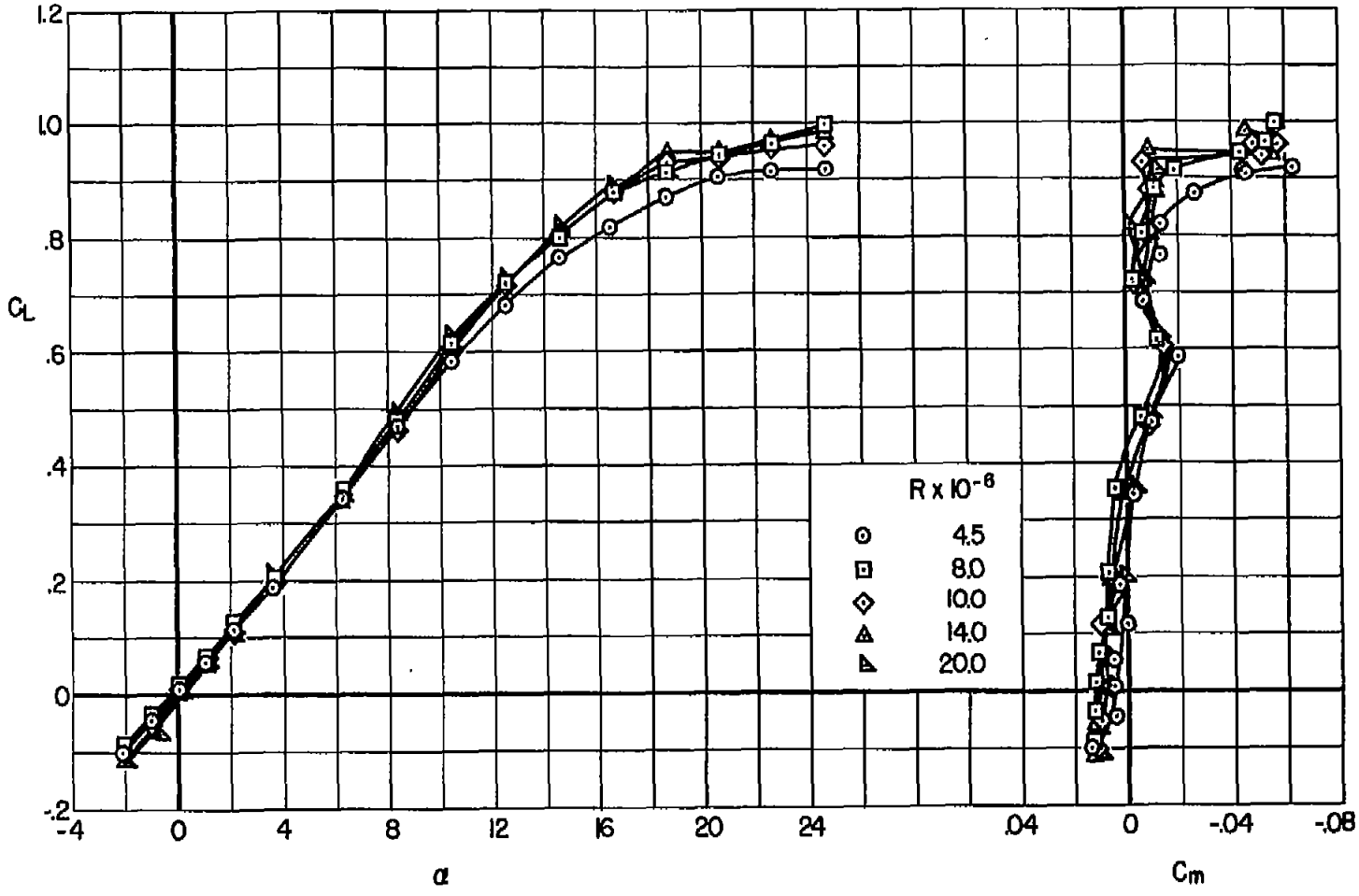

(a) C_L vs. α, C_m

Figure 12.- Low-speed aerodynamic characteristics of the basic large-scale model, without the vertical tail, at various Reynolds numbers.

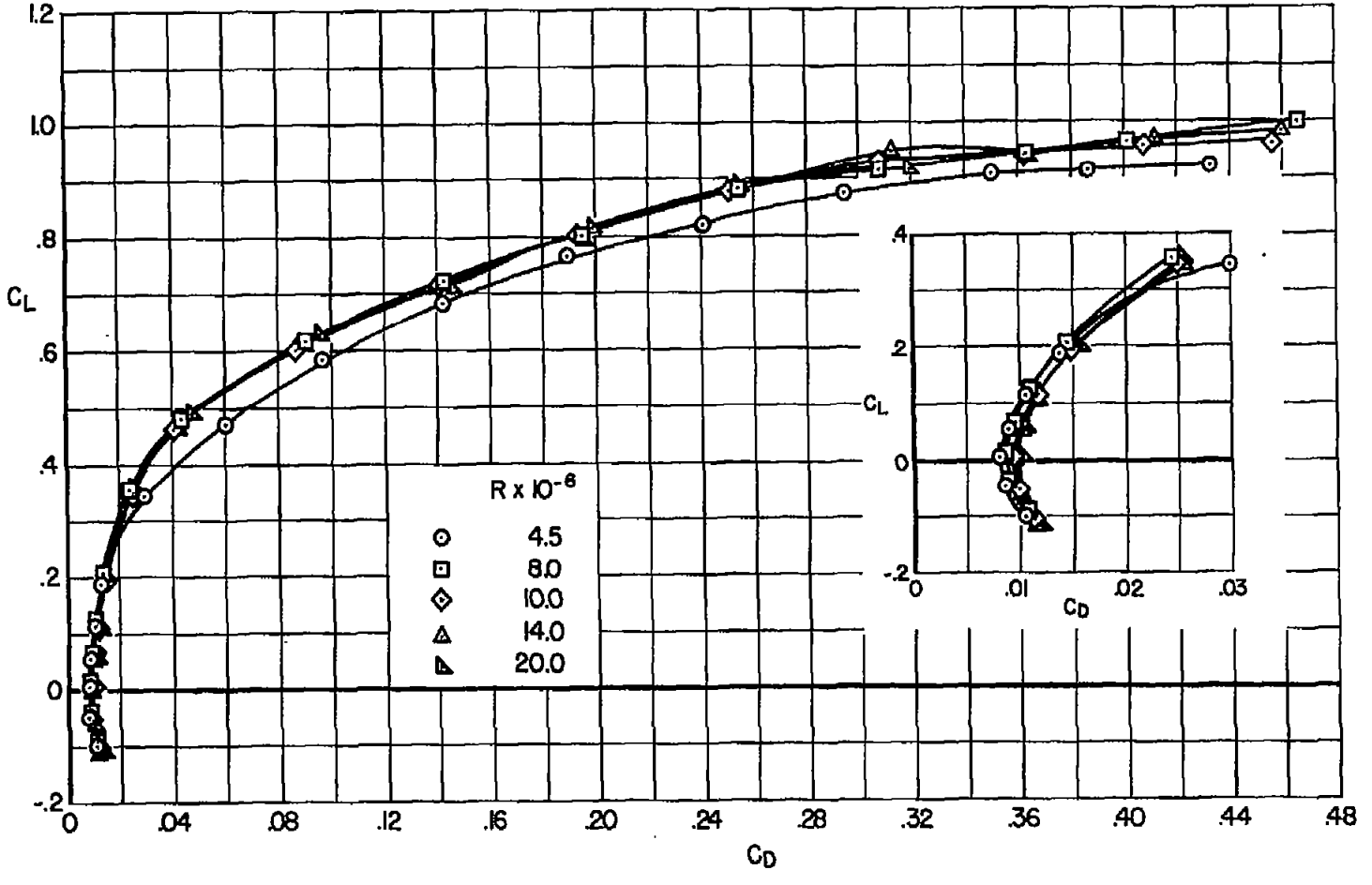

(b) C_L vs. C_D

Figure 12.- Concluded.

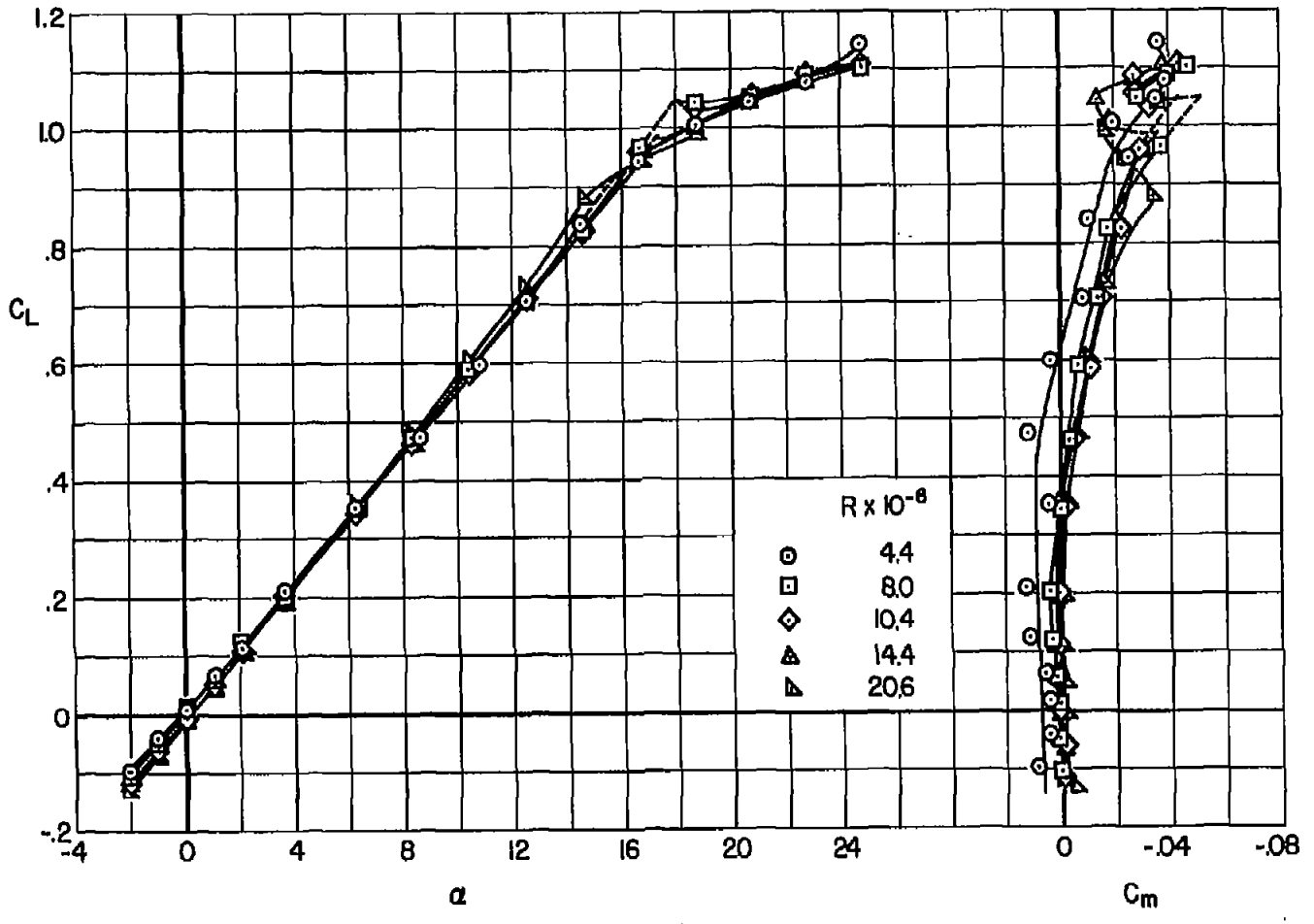

(a) C_L vs. α, C_m

Figure 13.- Low-speed aerodynamic characteristics of the modified large-scale model, without the vertical tail, at various Reynolds numbers.

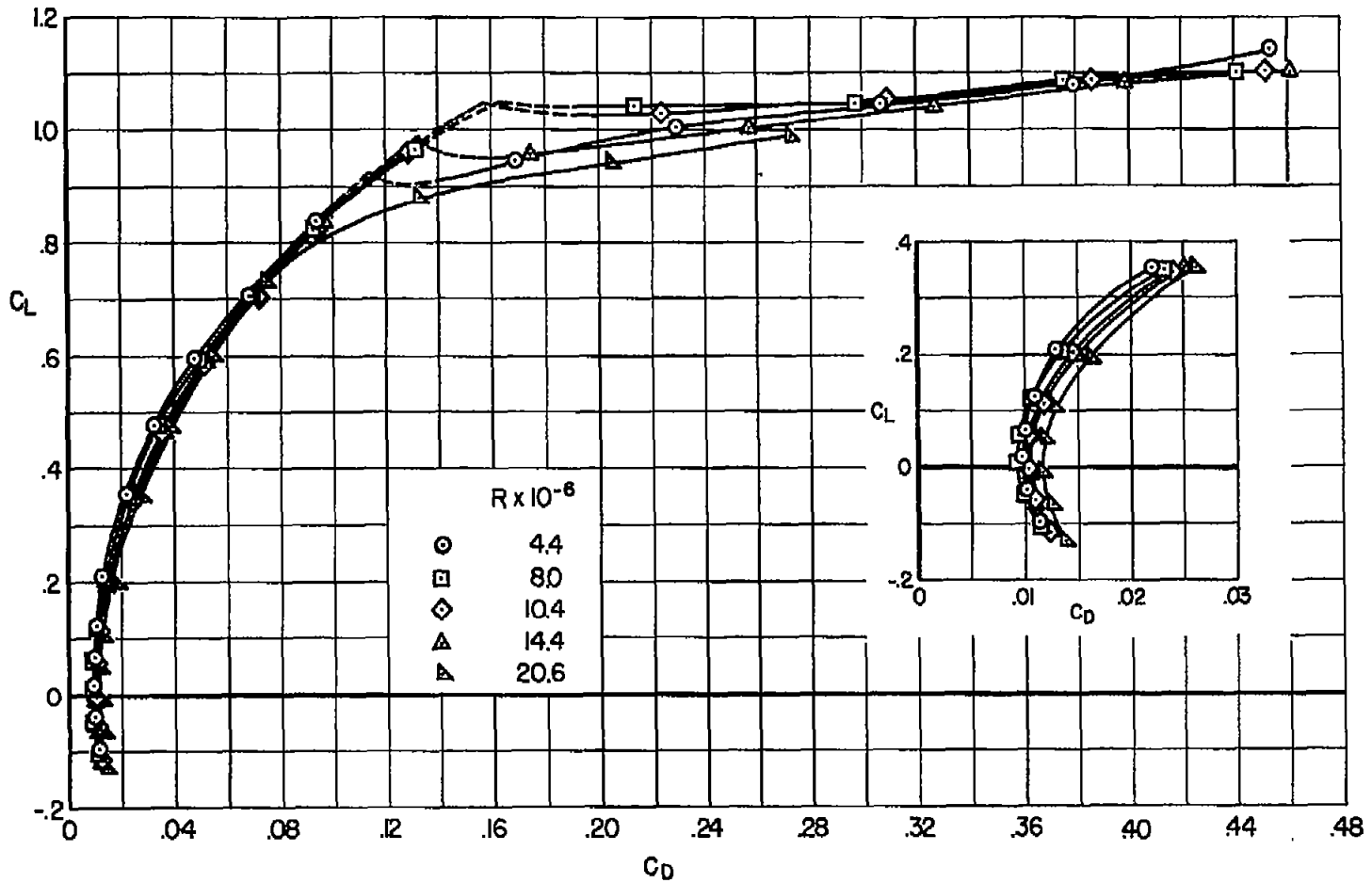

(b) C_L vs. C_D

Figure 13.- Concluded.

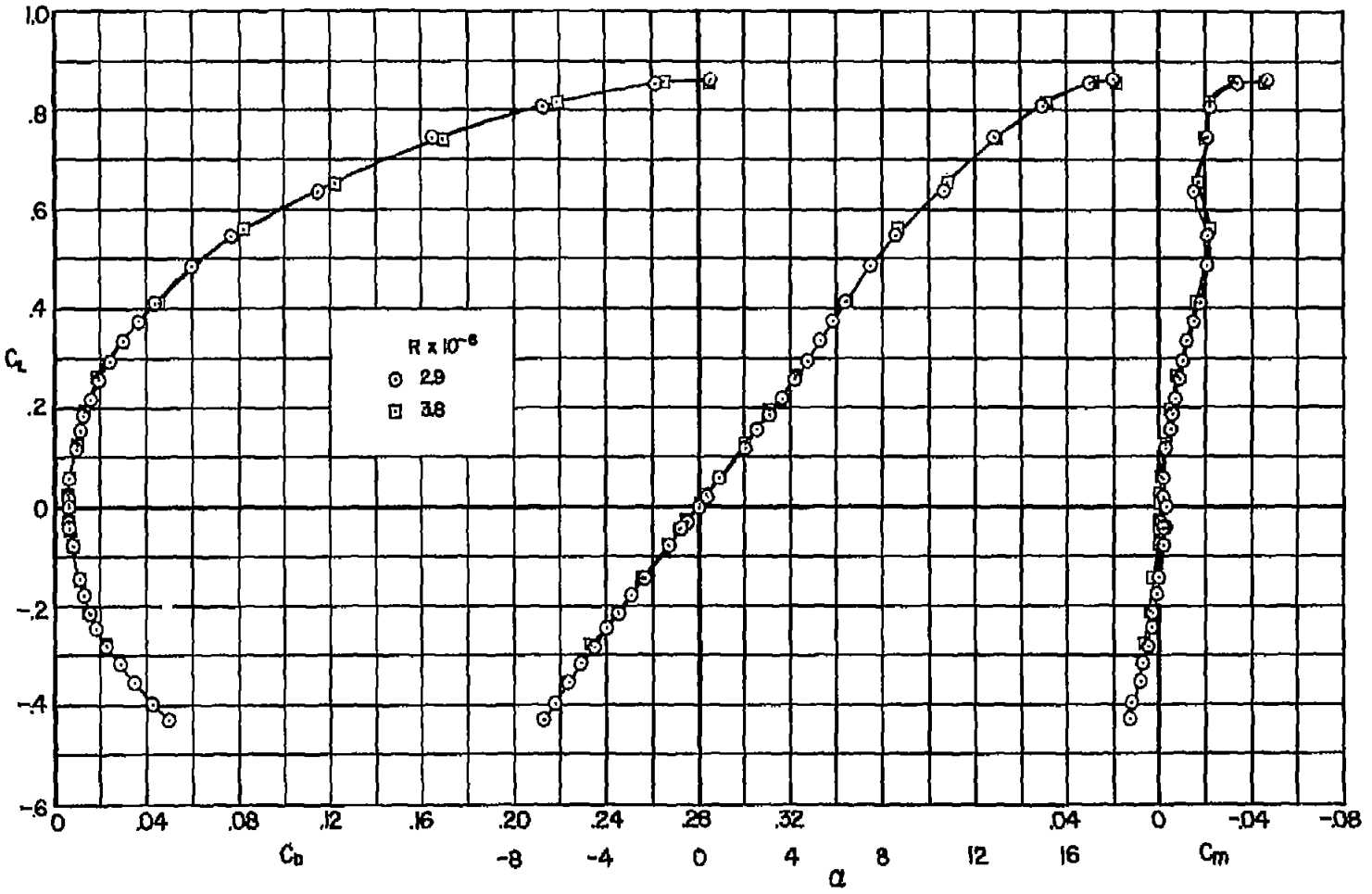

(a) M = 0.6

Figure 14.- High-subsonic-speed aerodynamic characteristics of the basic small-scale model at various Reynolds numbers.

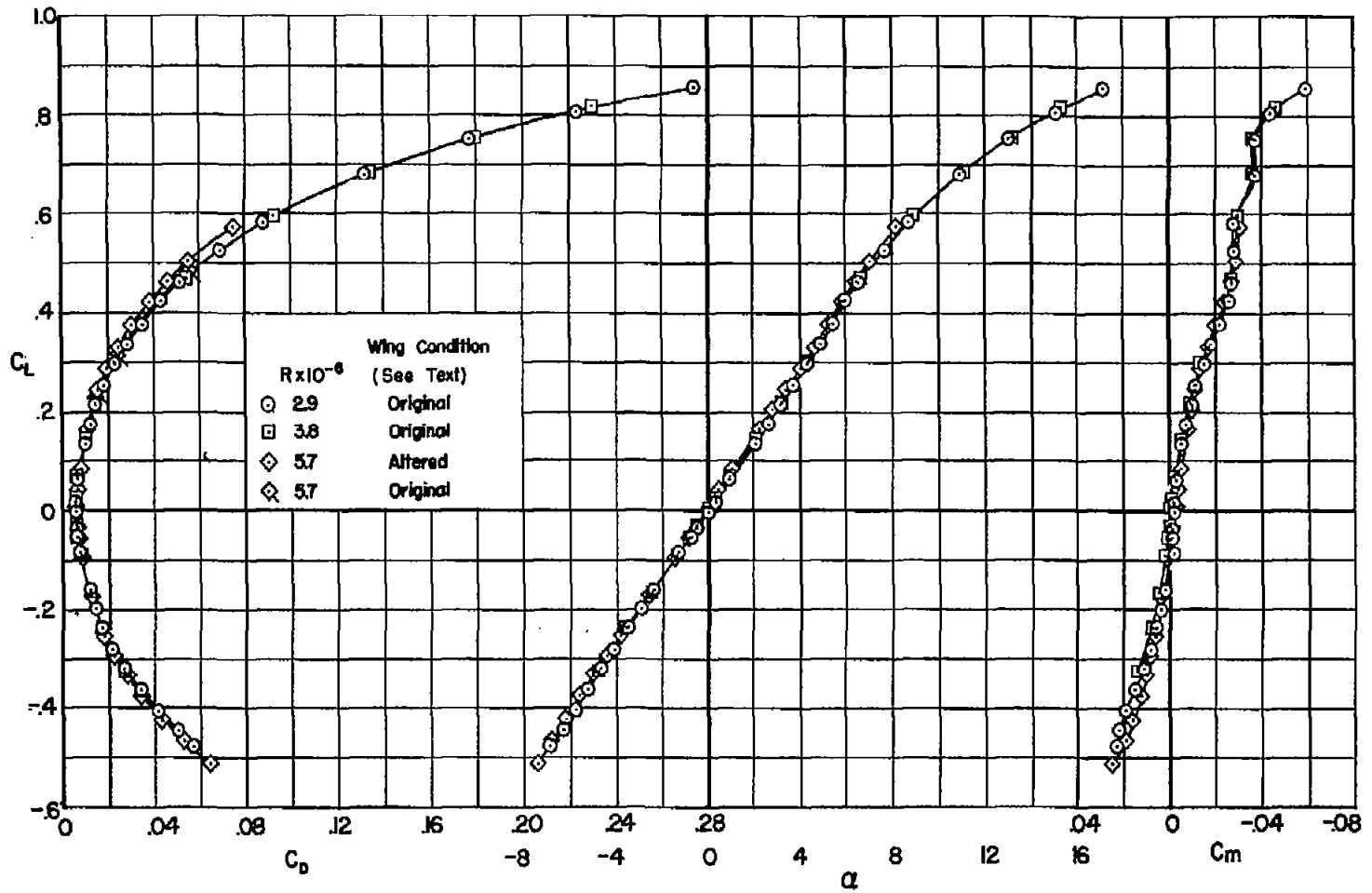

(b) M = 0.8

Figure 14.- Continued.

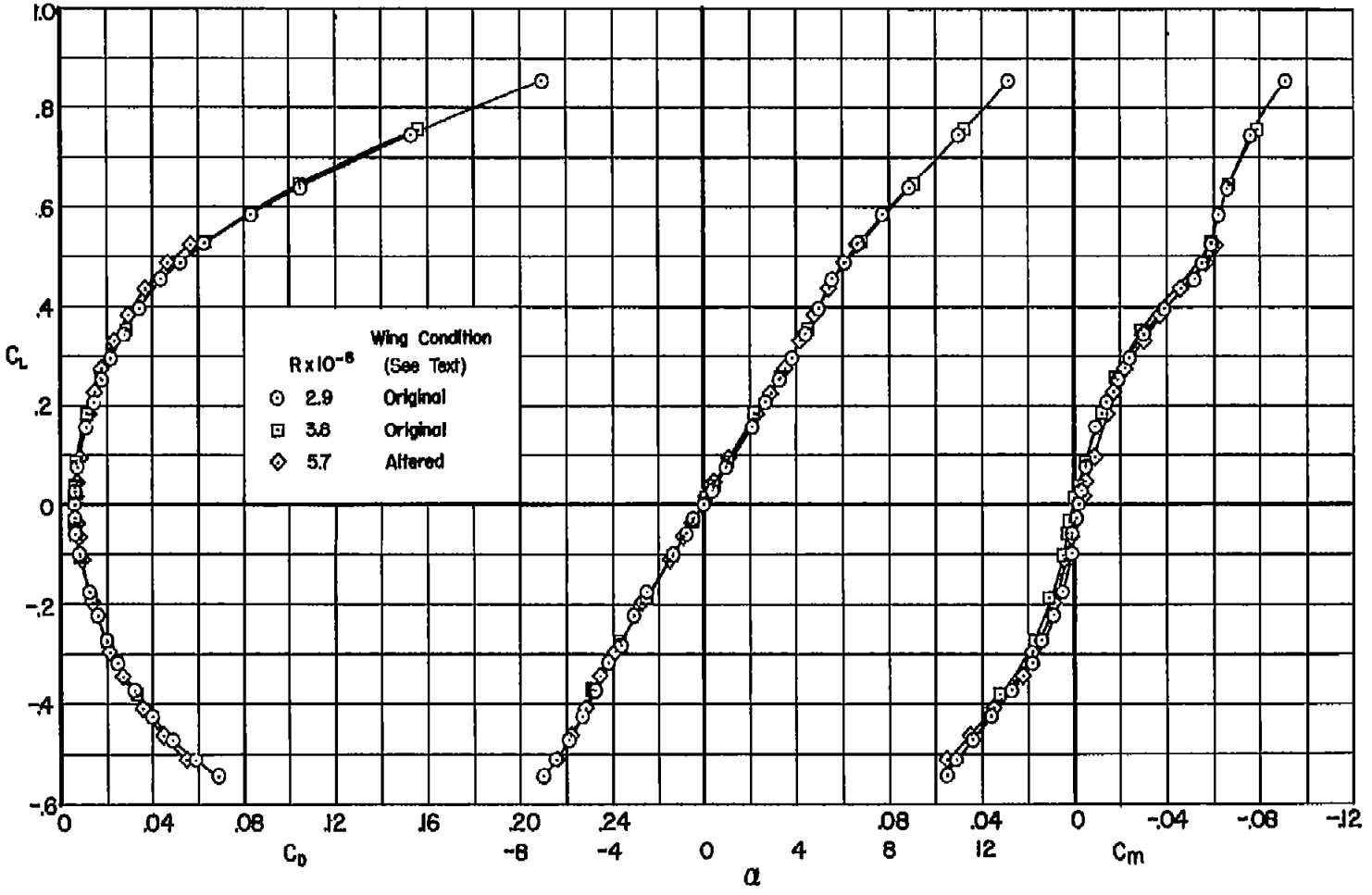

(c) M = 0.9

Figure 14.- Concluded.

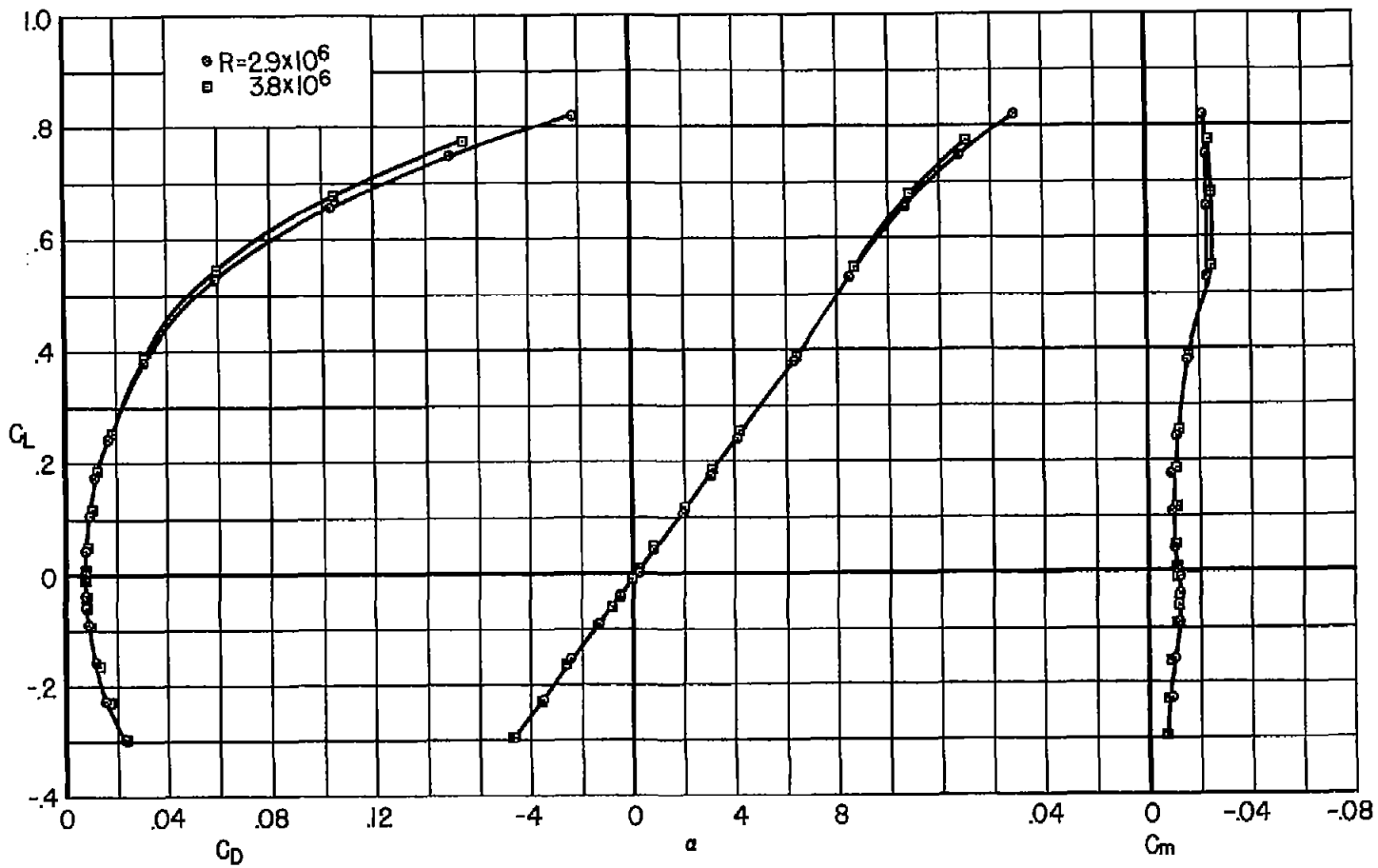

(a) M = 0.6

Figure 15.- High-subsonic-speed aerodynamic characteristics of the modified small-scale model at various Reynolds numbers.

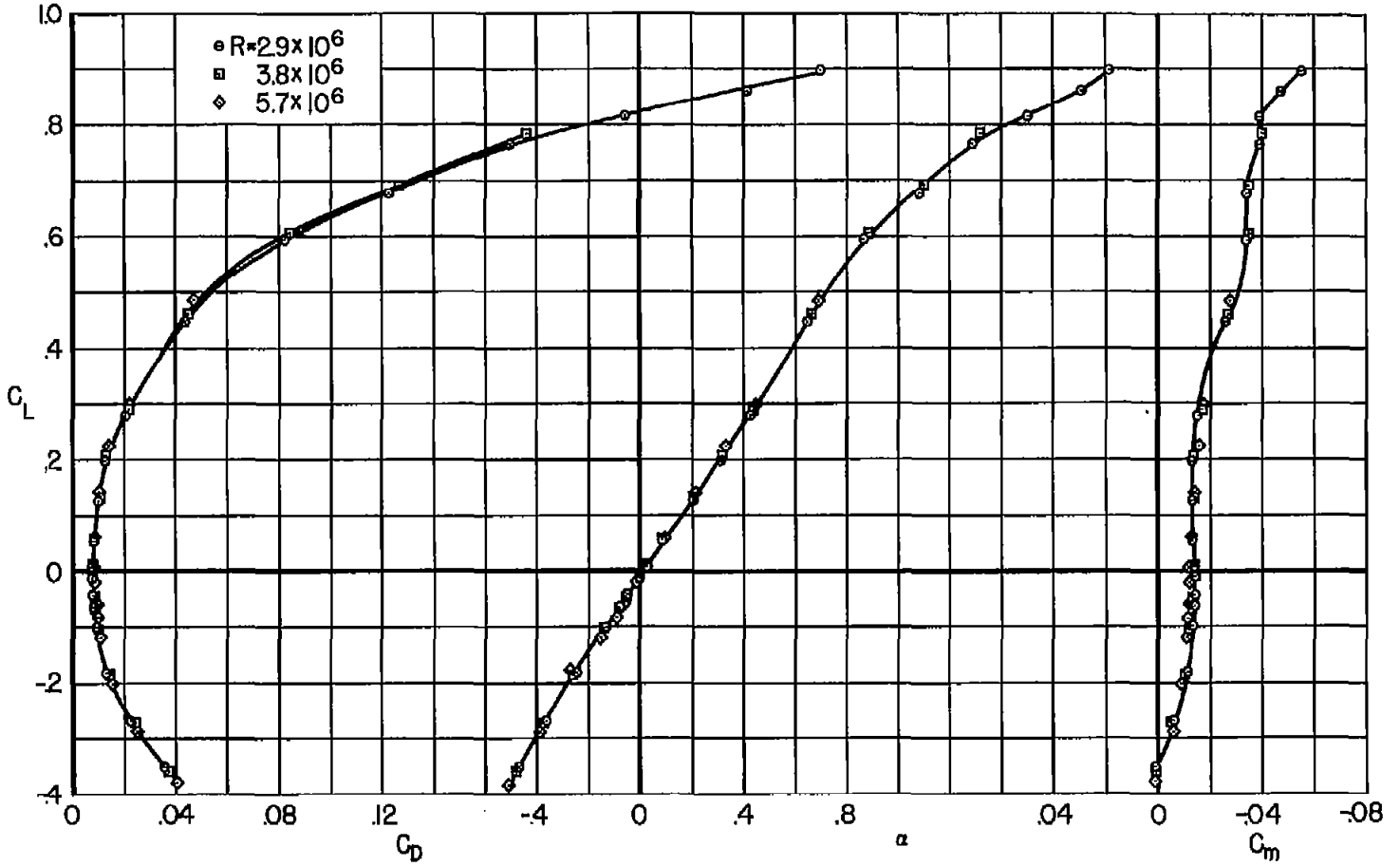

(b) M = 0.8

Figure 15.- Continued.

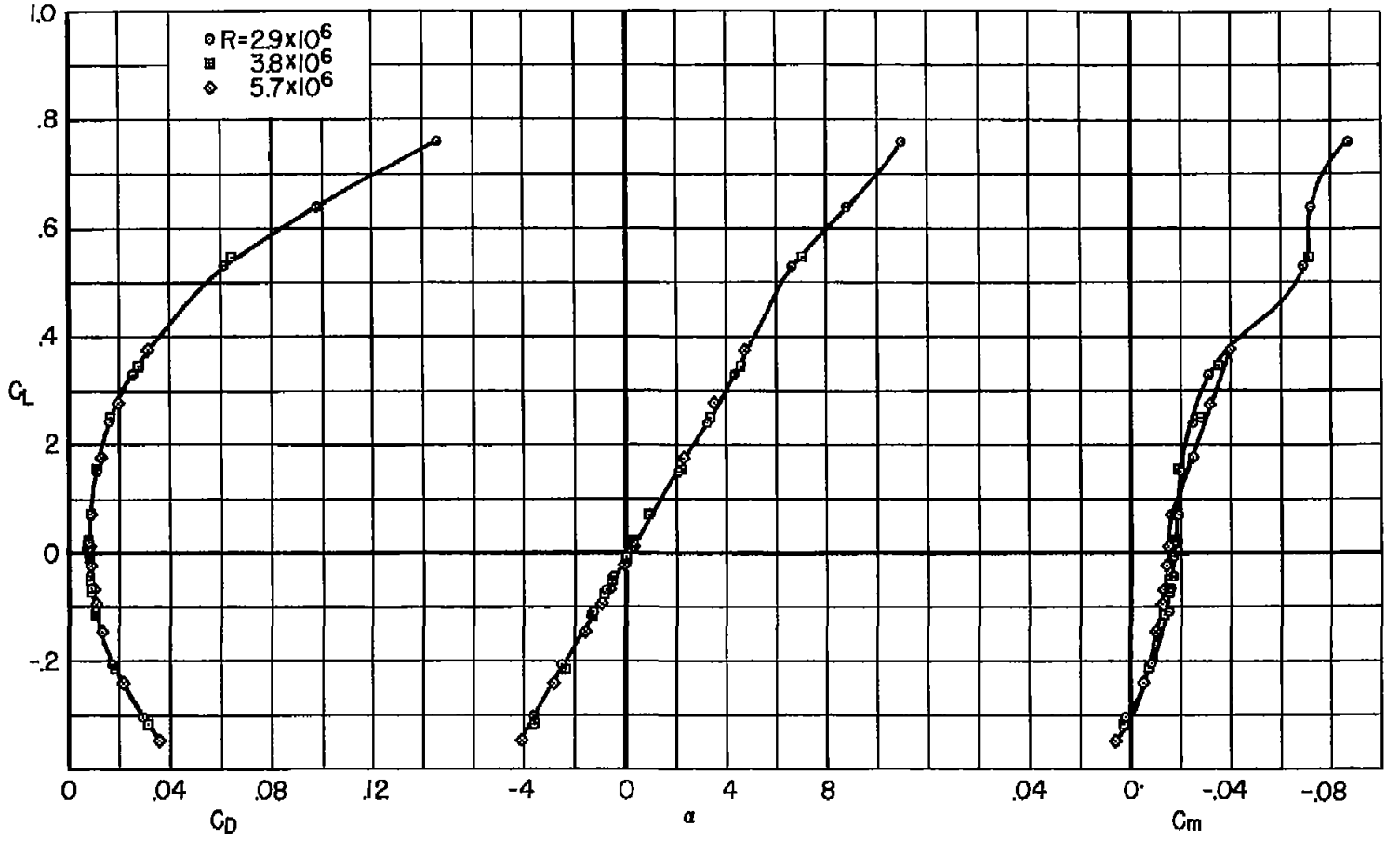

(c) M = 0.9

Figure 15.- Concluded.

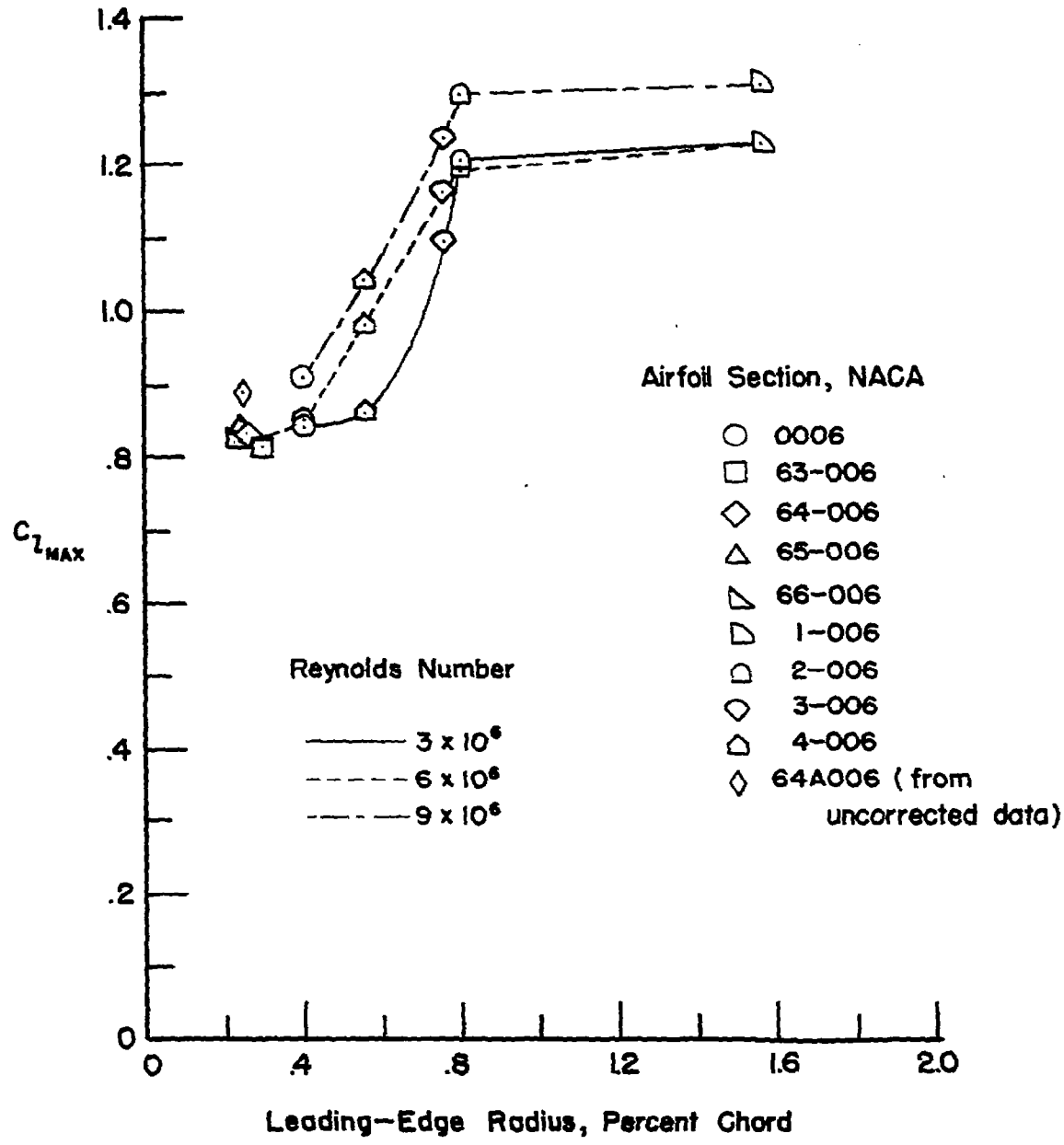

Figure 16.- Effect of leading-edge radius on maximum lift at low speeds of symmetrical 6-percent-thick airfoil sections.

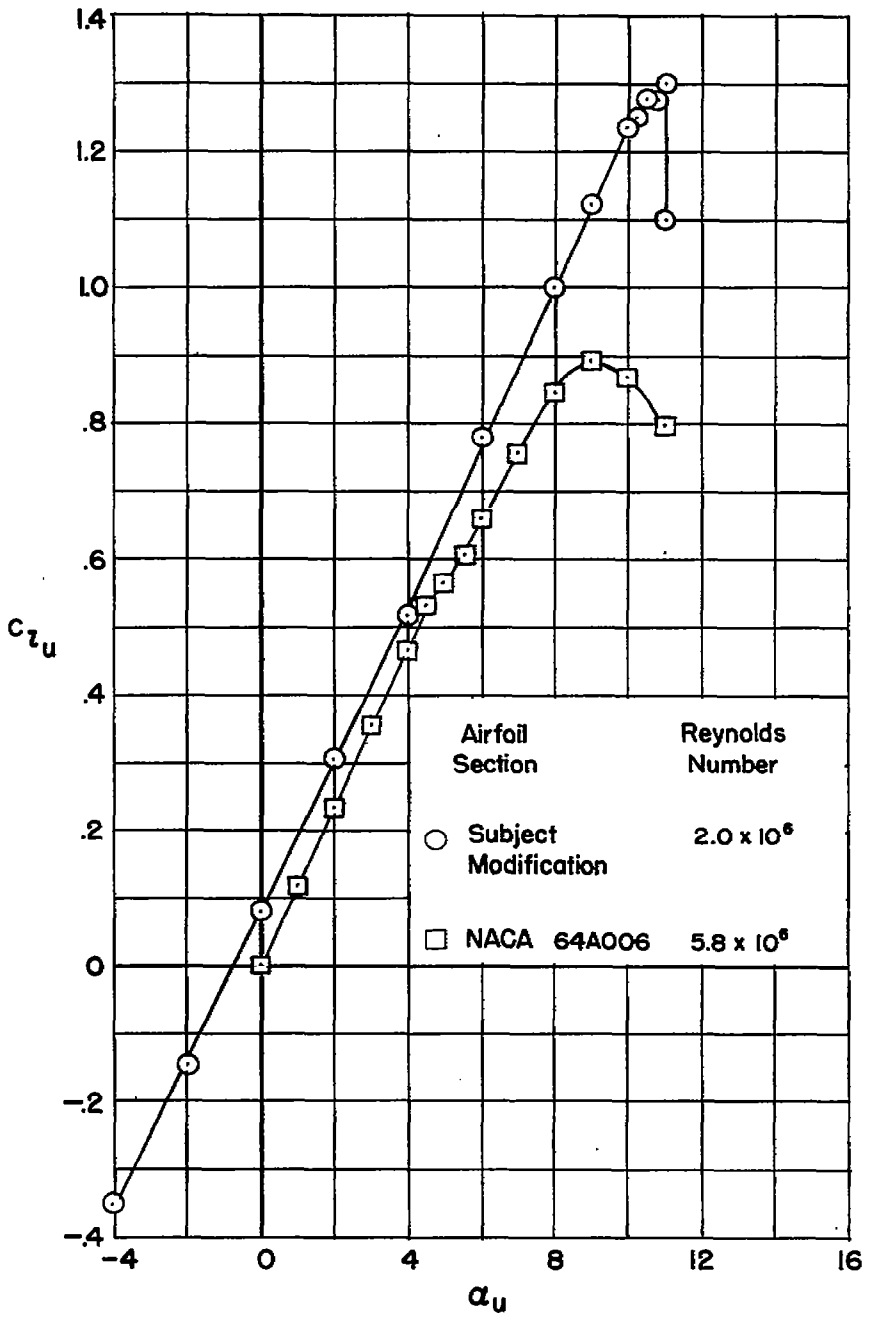

Figure 17.- Two-dimensional lift curves for the modified airfoil section and for the NACA 64A006 airfoil section, the latter taken from reference 9.